Journal of Medicinal Chemistry

Article

Synthesis and Pharmacological Characterization of C4-(Thiotriazolyl)-Substituted-2-Aminobicyclo[3.1.0]hexane-2,6-Dicarboxylates. Identification of (1R,2S,4R,5R,6R)-2-Amino-4-(1H-1,2,4-triazol-3-ylsulfanyl)bicyclo[3.1.0]hexane-2,6-dicarboxylic acid (LY2812223), a Highly Potent, Functionally Selective mGlu2 Receptor Agonist

James A Monn, Lourdes Prieto, Lorena Taboada, Junliang Hao, Matt R Reinhard, Steven S. Henry, Christopher D. Beadle, Lesley Walton, Teresa Man, Helene Rudyk, Barry Clark, David Tupper, S. Richard Baker, Carlos Lamas, Carlos Montero, Alicia Marcos, Jaime Blanco, Mark Bures, David K. Clawson, Shane Atwell, Frances Lu, Jing Wang, Marijane Russell, Beverly A Heinz, Xushan Wang, Joan H. Carter, Brian G. Getman, John T. Catlow, Steven Swanson, Bryan G. Johnson, David B. Shaw, and David L. McKinzie

J. Med. Chem., **Just Accepted Manuscript** • DOI: 10.1021/acs.jmedchem.5b01124 • Publication Date (Web): 27 Aug 2015

ACS Publications

Journal of Medicinal Chemistry is published by the American Chemical Society. 1155 Sixteenth Street N.W., Washington, DC 20036

	Russell, Marijane; Eli Lilly and Company, Heinz, Beverly; Eli Lilly and Company, Quantitative Biology Wang, Xushan; Eli Lilly and Company, Quantitative Biology Carter, Joan; Eli Lilly and Company, Quantitative Biology Getman, Brian; Eli Lilly and Company, Quantitative Biology Catlow, John; Eli Lilly and Company, Drug Disposition Swanson, Steven; Eli Lilly and Company, Drug Disposition Johnson, Bryan; Eli Lilly and Company, Neuroscience Research Shaw, David; Eli Lilly and Company, Neuroscience Research McKinzie, David; Eli Lilly and Company, Neuroscience Research

Synthesis and Pharmacological Characterization of C4-(Thiotriazolyl)-Substituted-2-Aminobicyclo[3.1.0]hexane-2,6-Dicarboxylates. Identification of (1*R*,2*S*,4*R*,5*R*,6*R*)-2-Amino-4-(1*H*-1,2,4-triazol-3-ylsulfanyl)bicyclo[3.1.0]hexane-2,6-dicarboxylic acid (LY2812223), a Highly Potent, Functionally Selective $mGlu_2$ Receptor Agonist

James A. Monn,[ϕ*] Lourdes Prieto,[ϕ] Lorena Taboada,[ϕ] Junliang Hao,[ϕ] Matthew R. Reinhard,[ϕ] Steven S. Henry,[ϕ] Christopher D. Beadle,[ϕ] Lesley Walton,[ϕ] Teresa Man,[ϕ] Helene Rudyk,[ϕ] Barry Clark,[ϕ] David Tupper,[ϕ] S. Richard Baker,[ϕ] Carlos Lamas,[ϕ] Carlos Montero,[ϕ] Alicia Marcos,[ϕ] Jaime Blanco,[ϕ] Mark Bures,[ϕ] David K. Clawson,[‡] Shane Atwell,[‡] Frances Lu,[‡] Jing Wang,[‡] Marijane Russell,[‡] Beverly A. Heinz,[†] Xushan Wang,[†] Joan H. Carter,[†] Brian G. Getman,[†] John T. Catlow,[†] Steven Swanson,[†] Bryan G. Johnson,[§] David B. Shaw,[§] and David L. McKinzie[§]

[ϕ]Discovery Chemistry Research and Technologies, [†]Quantitative Biology, [‡]Structural Biology, [†]Drug Disposition and [§]Neuroscience Research, Eli Lilly and Company, Indianapolis, IN 46285.

Abstract:

Identification of orthosteric $mGlu_{2/3}$ receptor agonists capable of discriminating between individual $mGlu_2$ and $mGlu_3$ subtypes has been highly challenging owing to the glutamate-site sequence homology between these proteins. Herein we detail the preparation and characterization of a series of molecules related to 1*S*,2*S*,5*R*,6*S*-2-aminobicyclo[3.1.0]hexane-2,6-dicarboxylate **1** (LY354740) bearing C4-thiotriazole substituents. Based on second messenger responses in cells expressing recombinant human $mGlu_{2/3}$ subtypes, a number of high potency and efficacy $mGlu_2$ receptor agonists exhibiting low potency $mGlu_3$ partial agonist / antagonist activity were identified. From this, (1*R*,2*S*,4*R*,5*R*,6*R*)-2-Amino-4-(1*H*-1,2,4-triazol-3-ylsulfanyl)bicyclo[3.1.0]hexane-2,6-dicarboxylic acid **14a** (LY2812223) was further characterized. Co-crystallization of **14a** with the amino terminal domains of $hmGlu_2$ and $hmGlu_3$ combined with site-directed mutation studies has clarified the underlying molecular basis of this unique pharmacology. Evaluation of **14a** in a rat model responsive to $mGlu_2$ receptor activation coupled with a measure of central drug disposition provides evidence that this molecule engages and activates central $mGlu_2$ receptors in vivo.

Introduction

Metabotropic glutamate (mGlu) receptors are members of the family C subgroup of the seven-transmembrane (7-TM) domain receptor superfamily. The mGlu receptors have attracted considerable attention as targets for small molecule-based therapeutic interventions in both central nervous system (CNS) and non-CNS disorders.[1] Of the eight known mGlu subtypes ($mGlu_{1-8}$), $mGlu_2$ and $mGlu_3$ receptors are among the most extensively studied owing to both the availability of potent and selective small molecule orthosteric agonists, orthosteric antagonists and allosteric modulators (both positive and negative) and to the robust physiologic effects produced by many of these ligands in preclinical models of psychiatric (e.g. anxiety, depression, schizophrenia and addiction),[2] neurologic (e.g. neuropathic pain and neurodegeneration),[3] and proliferative (e.g. glioma)[4] disorders. Interest in identifying molecules that elicit or enhance $mGlu_{2/3}$ receptor signaling has been the subject of particular interest owing to clinical evidence demonstrating beneficial effects of $mGlu_{2/3}$ receptor agonists **1**[5] and **2**[6] (Figure 1; dosed as oral prodrug forms **3** and **4**) in generalized anxiety disorder[7] and schizophrenia[8] patients, respectively. Though the efficacy of **4** in chronic schizophrenia patients was not confirmed in subsequent clinical trials,[9a,b] an antipsychotic response in patient subgroups was noted.[9b-d]

Figure 1. Clinically evaluated $mGlu_{2/3}$ receptor agonists (**1** and **2**) and their orally bioavailable prodrugs (**3** and **4**).

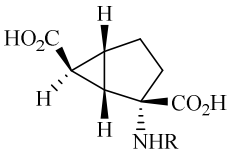

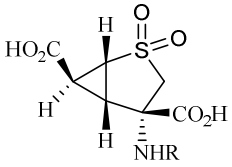

1: R = H **2**: R = H
3: R = L-Alanine **4**: R = L-Methionine

Owing to their high degree of sequence homology, overlapping orthosteric agonist and antagonist pharmacology and common signal transduction mechanisms, $mGlu_2$ and $mGlu_3$ receptors have historically been clustered together (i.e. group II mGluRs). However, these two signaling molecules are differentially localized in the central nervous system (CNS)[10] and have divergent functions. For instance, while both $mGlu_2$ and $mGlu_3$ receptors appear to play a role in anti-stress effects produced by $mGlu_{2/3}$ agonists in rodents,[11] $mGlu_2$ receptors appear to mediate

both the acute antipsychotic[12] and antinociceptive[13] responses to $mGlu_{2/3}$ agonists in animal models of psychosis and pain, while activation of glial $mGlu_3$ receptors mediates $mGlu_{2/3}$ agonist-elicited neuroprotection via mechanisms involving increased glutamate transporter protein expression[14,15c] and the release of trophic factors including GDNF and TGF_{β}.[15] Finally, post-synaptically localized $mGlu_3$ receptors appear to enhance network activity and induce theta oscillations in the hippocampus[16] as well as to trigger long term depression in the prefrontal cortex,[17] mechanisms which may have therapeutic implications for the treatment of thought disorders and the extinguishing of fear memories. Elucidation of $mGlu_2$ vs. $mGlu_3$ receptor function in these studies has been primarily enabled by the use of murine lines in which embryonic deletions of the genes encoding $mGlu_2$ and/or $mGlu_3$ receptors were employed. While these biological reagents are useful for validating the roles of specific proteins in physiologic and pathophysiologic processes and for establishing the mechanism(s) of small and large molecule ligands, compensatory changes can occur over the course of development, potentially confounding the interpretation of biological studies. For example, deletion of the gene encoding $mGlu_2$ receptors led to increased hippocampal expression of both $mGlu_3$ and NMDA receptor subunit NR2A and a decrease in expression of the glutamate transporter EAAT3, while deletion of the gene encoding $mGlu_3$ receptors resulted in the increased hippocampal expression of both $mGlu_2$ and NR2A and decreased expression of glutamate transporters (EAAT1/2).[18] Therefore, in order to more firmly establish the roles of $mGlu_2$ and $mGlu_3$ receptor subtypes in CNS disorders, it is of continued interest to identify potent pharmacological tools that are capable of differentiating these receptors in both in vitro and in vivo systems.

The primary amino acid sequences for both $mGlu_2$ and $mGlu_3$ receptors are known.[19] Furthermore, crystal structures of the amino terminal domain (ATD) segments of both rat (with agonists)[20a] and human (with an antagonist)[20b] $mGlu_3$ receptors have been described. Owing to the high degree of protein sequence homology between these two receptor subtypes, especially those residues involved in glutamate binding (Table 1), identification of glutamate-site (orthosteric) agonists or antagonists capable of differentiating between these receptor subtypes has been an extremely challenging endeavor.

Table 1. Full length and sub-domain homology between $mGlu_2$ and $mGlu_3$ receptors

	$mGlu_2$ vs. $mGlu_3$	
Protein Segment	% Identity	% Homology
Full Length Receptor	67	81
7-Transmembrane (7-TM) Domain	71	84
Amino Terminal Domain	64	80
Glutamate-binding site residues[a,b]	100	100

[a]$mGlu_2$: R57, R61, K377, D295, T168, S145, A166, S143
[b]$mGlu_3$: R64, R68, K389, D301, T174, S151, A172, S149

Indeed, while many positive allosteric modulators (PAMs) which bind within the 7-TM domain of $mGlu_2$ have been identified[21], only two examples of orthosteric agonists (**5** and **6,** Figure 2) capable of selective $mGlu_2$-receptor activation have been described. Of these, (1*S*,2*S*,4*R*,5*R*,6*S*)-2-amino-4-methylbicyclo[3.1.0]hexane-2,6-dicarboxylic acid, **5** (LY541850) displayed unusual $mGlu_2$ agonist (EC_{50} = 161 nM) and $mGlu_3$ antagonist (IC_{50} = 1 μM) activity[22] while **6** is reported to activate $mGlu_2$ with low potency (EC_{50} = 10 μM) but excellent selectivity over $mGlu_3$ (EC_{50} > 1000 μM).[23] Interestingly, expansion of the structure-activity relationship (SAR) for compounds substituted at the C4-position of **1** was not successful in identifying additional $mGlu_2$ receptor-selective agonists such as **5**, but instead led to the identification of multiple highly potent, pharmacologically blended $mGlu_{2/3}$ receptor agonists such as (1*R*,2*S*,4*R*,5*R*,6*R*)-2-amino-4-fluorobicyclo[3.1.0]hexane-2,6-dicarboxylic acid **7**, (LY459477, Figure 2)[24] and (1*R*,4*S*,5*S*,6*S*)-4-aminospiro[bicyclo[3.1.0]hexane-2,1'-cyclopropane]-4,6-dicarboxylic acid **8**, (LY2934747, Figure 2)[25] as well as low potency $mGlu_{2/3}$ antagonists (e.g. **9, 10**, Figure 2).[24] Moderate (2.25 – 2.3 Å) resolution co-crystal structures of the human $mGlu_2$ ATD with compounds **1** and **8**, and the human $mGlu_3$ ATD with compound **1** were recently used to more precisely understand agonist-receptor interactions and provided a rationale for the $mGlu_2$ agonist, $mGlu_3$ antagonist pharmacological profile of **5**.[25] In this account, we have extended our investigation of the effect of substituents attached to the C4-position of **1** on $mGlu_{2/3}$ receptor binding and function. Specifically, the present investigation has focused on the preparation and

evaluation of compounds in which substituted and unsubstituted thiotriazoles are attached to the $C4_{\alpha}$ and $C4_{\beta}$-positions of **1**. From this work we have identified a series of highly potent and efficacious $hmGlu_2$ receptor agonists that exhibit minimal $hmGlu_3$ agonist activity.

Figure 2. Selective and non-selective $mGlu_{2/3}$ receptor agonists and antagonists

---

Lower potency, pharmacologically-selective mGlu2 agonists

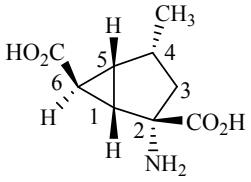

5[22]

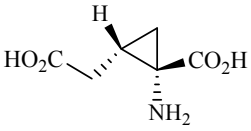

rac-**6**[23]

High potency, pharmacologically-balanced mGlu2/3 agonists

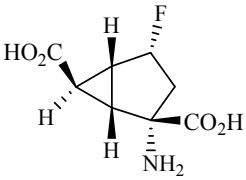

7[24]

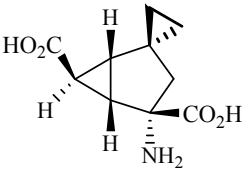

8[25]

Low potency, pharmacologically-balanced mGlu2/3 antagonists

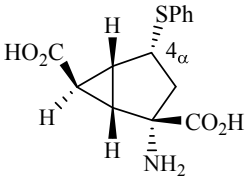

9[24]

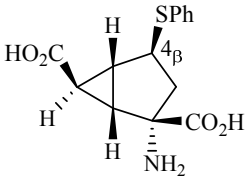

10[24]

Chemistry

Non-racemic C4$_\alpha$-substituted thiotriazoles (**14a-g**) were readily prepared from the previously described non-racemic C4$_\beta$-tosylate **11**[24] (Scheme 1) while non-racemic C4$_\beta$-substituted thiotriazoles (**16a-g***)* were prepared in an analogous manner from non-racemic C4$_\alpha$-bromide **12**[24] (Scheme 2). In each case, thiolate displacement of the C4-leaving group (OTs or Br) proceeded with inversion of configuration with yields ranging from 42-99%. Assignment of relative stereochemistry for intermediates **13a-g** and **15a-g** was made on the basis of the C4 proton splitting pattern in the ^{1}H-NMR spectrum. In all cases the C4 proton for α-substituted thiotriazoles **13a-g** is a multiplet while in β-substituted thiotriazoles **15a-g** the C4 proton appears as a doublet.[26] Removal of the amino acid protecting groups was achieved in a single step under a variety of conditions (e.g. $ZnBr_2$, HCl, or AcOH). The final products **14a-g**, **16a-g** were isolated as either HCl salts or neutral zwitterions (see experimental section for details). Confirmation of absolute and relative stereochemistry of one final product from this series (**14a**) was obtained from the structure of this compound co-crystalized with $hmGlu_2$ and $hmGlu_3$ amino terminal domain (ATD) proteins (see Figure 8). All final compounds were characterized by ^{1}H-NMR, ^{13}C-NMR and LCMS and judged to be >95% pure by capillary electrophoresis.

Scheme 1. Preparation of C4$_\alpha$-substituted thiotriazoles **14a-g**

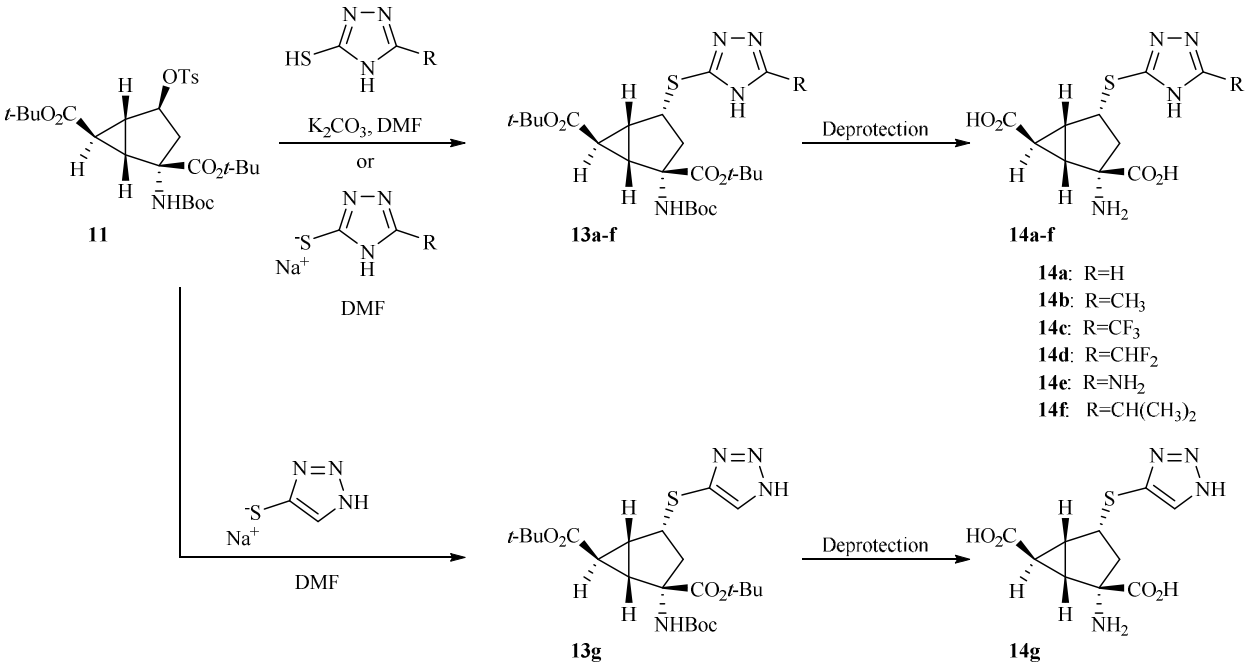

Scheme 2. Preparation of C4$_\beta$-substituted thiotriazoles **16a-g**

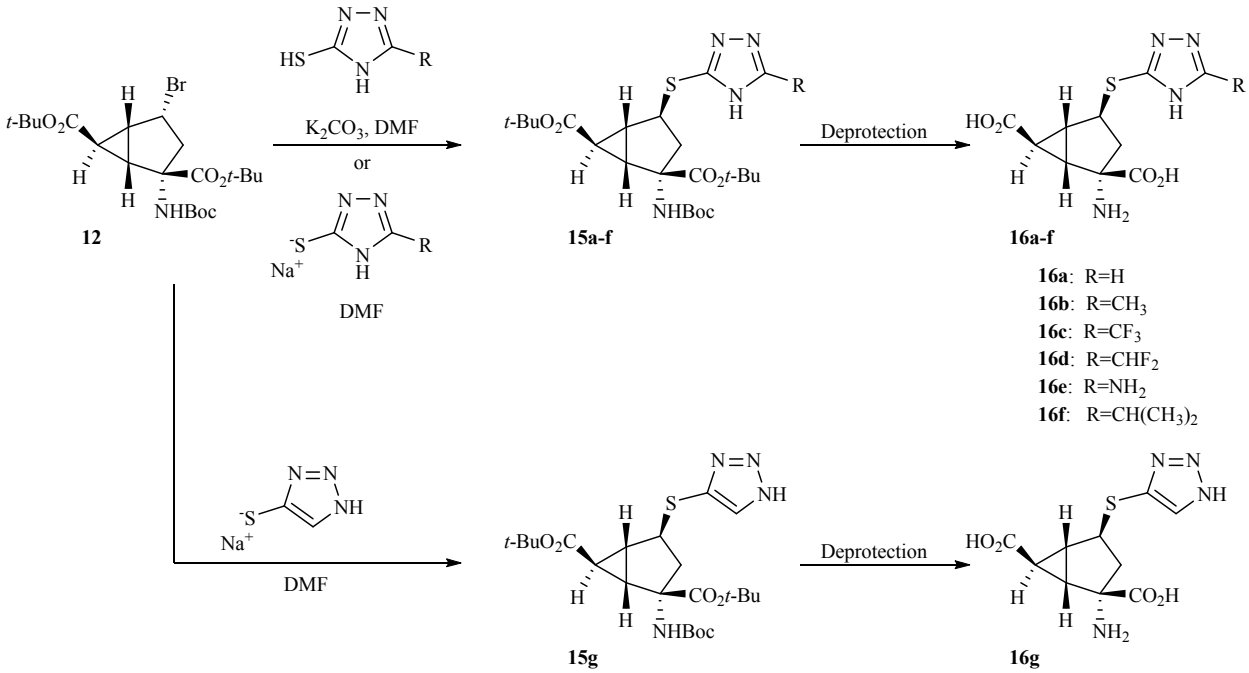

Results

$hmGlu_{2/3}$ receptor binding:[27] Compounds **14a-g**, **16a-g** along with comparators **1**, **9 and 10** were assessed for their ability to displace [^{3}H]-**7**[28] from membranes expressing recombinant human $mGlu_2$ or $mGlu_3$ receptors (Table 2). Across the entire series, $mGlu_2$ and $mGlu_3$ Ki values were poorly correlated with each other (r^2 = 0.29, supporting information Figure S1). Analogs bearing $C4_\alpha$-thiotriazole substituents (**14a-g**) exhibited a limited range of binding affinities at both $hmGlu_2$ (Ki values ranged from 67.0 nM for **14e** to 266 nM for **14f**) and $hmGlu_3$ (Ki values ranging from 56.7 nM for **14c** to 259 nM for **14g**) with no remarkable (i.e. within 10x) loss or improvement of affinity over either the unsubstituted analog **1** or $C4_\alpha$-thiophenylether **9**. Furthermore, $C4_\alpha$-substituted compounds **14a-g** did not exhibit a notable difference in binding affinities between $hmGlu_2$ and $hmGlu_3$ receptors (affinity ratios were within 2-fold between these two receptors across the series). Conversely, analogs bearing $C4_\beta$-thiotriazole substituents (**16a-g**) exhibited a considerable dynamic range of binding affinities for $hmGlu_2$ (Ki values ranging from 8.55 nM for **16c** to 339 nM for **16f**), while the range in the affinities of **16a-g** for $hmGlu_3$ was relatively narrow (Ki values ranging from 43.1 nM for **16c** to 126 nM for **16a**). Enhanced $mGlu_2$ receptor affinity for certain members of the current series compared to both unsubstituted analog **1** and $C4_\beta$-thiophenylether **10** was apparent. Noteworthy in this regard was the nearly 150-fold improvement in $mGlu_2$ binding affinity for **16c** (Ki = 8.55 nM) over **10** (Ki = 1,230 nM). As was observed for $C4_\alpha$-substituted analogs **14a-g**, individual $C4_\beta$-substituted analogs **16a-g** exhibited no particular binding preference for one receptor subtype over the other, demonstrating $mGlu_{2/3}$ affinity ratios for individual molecules within 5-fold across the series. The effect of C4-stereochemistry on binding affinity for otherwise identically substituted analogs (i.e. comparing matched pairs of **14a-g** and **16a-g**) varied. Diastereomers **14c** and **16c** (4-CF_3 substituted triazoles) demonstrated the greatest difference in binding affinities (10-fold at $mGlu_2$ favoring the $C4_\beta$-isomer) while most other isomeric pairs showed only modest (1-3 fold) differences in Ki values.

Table 2. Binding affinities and functional agonist or *antagonist* responses for C4-substituted analogs in cells expressing recombinant human $mGlu_2$ and $mGlu_3$ receptors[a]

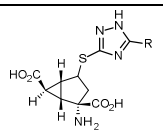		Inhibition of ^{3}H-459477 binding to human mGlu receptors Ki (nM) ± SEM		Functional agonist or *antagonist* activity in cells expressing recombinant human mGlu receptors EC_{50} (nM) or *IC_{50} (nM)* ± SEM (Emax[b] or *Imax*)			
R	No.	$mGlu_2$	$mGlu_3$	$mGlu_2$		$mGlu_3$	
				cAMP[c]	Ca^{2+} FLIPR[d]	cAMP[c]	Ca^{2+} FLIPR[d]
H	**1**	71.7 ± 5.9	107 ± 12.5	7.0 ± 1.2 (100%)	34.4 ± 4.01 (94)	27.9 ± 3.0 (100%)	140 ± 4.6 (103%)
SPh	**9**	420 ± 30.3	138 ± 15.3	*7000± 645[e] (80)*	>12500 *>12500*	>25000 *1070 ± 258 (92)*	>25000 *7690 ± 7260 (62)*
SPh	**10**	1230 ± 139	272 ± 25.1	1170 ± 232 (49) *15300± 5400 (53)*	>25000 *>12500*	>25000 *3370 ± 1210 (77)*	>5000 *6710 (n=2) (56)*
H	**14a**	144 ± 20.0	156 ± 23.5	5.6 ± 0.5 (99)	21.1 ± 2.2 (95)	129 ± 34.9 (61) *2730 ± 1430 (40)*	>25000 *25200 ± 15600 (58)*
Me	**14b**	121 ± 34.3	62.4 ± 12.6	10.4 ± 1.8 (99)	39.5 ± 7.5 (100)	103 ± 13 (77)	105 ± 78 (49)
CF_3	**14c**	84.4 ± 13.3	56.7 ± 8.86	13.9 ± 2.6 (99)	54.2 ± 6.3 (82)	79.5 ± 18.7 (66) *528± 99.4 (46)*	82.0 ± 49.6 (37)
CHF_2	**14d**	95.8 ± 9.35	63.2 ± 9.37	11.8 ± 0.3 (98)	53.6 ± 13.7 (82)	77.7 ± 14 (60) *459 ± 209 (33)*	>25000 *154 ± 34.4 (71)*
NH_2	**14e**	67.0 ± 8.11	58.3 ± 9.11	4.5 ± 0.2 (100)	13.0 ± 2.6 (100)	74 ± 11.1 (77)	>25000 *94.7 ± 18.9 (80)*
iPr	**14f**	266 ± 60.3	157 ± 33.8	16.5 ± 4.5 (100)	87.8 ± 6.6 (89)	281 ± 63.3 (67) *859 ± 340 (59)*	>25000 *>12500 (47)*
123Triaz[f]	**14g**	142 ± 18.0	259 ± 20.6	12.4 ± 1.4 (99)	46.1 ± 17.6 (92)	235 ± 37.2 (69) *2380 ± 1270 (49)*	>25000 *5510 ± 1860 (63)*
H	**16a**	60.4 ± 6.20	126 ± 14.5	11.2 ± 1.3 (99)	69.1 ± 21.9 (89)	227 ± 39.1 (52) *4260 ± 4090 (54)*	>25000 *3100 ± 170 (72)*
Me	**16b**	171 ± 16.7	79.0 ± 9.4	44.3 ± 5.5 (99)	146 ± 24.3 (84)	96.6 ± 28.8 (74)	>25000 *3590 (57, n=1)*
CF_3	**16c**	8.55 ± 1.63	43.1 ± 14.1	0.65 ± 0.07 (100)	7.8 ± 1.6 (99)	30.5 ± 4.1 (83)	>25000 *624 ± 473 (61)*
CHF_2	**16d**	13.4 ± 2.55	57.5 ± 12.1	0.58 ± 0.06 (100)	6.3 ± 1.9 (95)	27.3 ± 8.8 (80)	>25000 *244 ± 90.8 (79)*
NH_2	**16e**	27.8 ± 2.92	69.0 ± 10.7	6.4 ± 1.0 (99)	20.1 ± 4.2 (100)	112 ± 25.4 (68)	>25000 *3870 ± 1490 (62)*

iPr	**16f**	339 ± 41.0	82.7 ± 3.78	74.0 ± 6.5 (99)	242 ± 27.5 (71)	77.9 ± 7.0 (87)	>25000 *2350 ± 1690 (62)*
123Triaz[f]	**16g**	111 ± 14.0	65.1 ± 5.87	5.2 ± 1.5 (98)	19.0 ± 0.9 (94)	92.7 ± 21.9 (81)	>25000 *2790 ± 1170 (67)*

[a]See experimental section for assay details; [b]Maximal response achieved compared to glutamate (100%); [c] $hmGlu_2$ B_{max} = 21859 fmol/mg protein, $hmGlu_3$ B_{max} = 5271fmol/mg protein. Agonist activity assessed as an inhibition of forskolin-stimulated cAMP, antagonist activity assessed as a reversal of DCG-IV-inhibited, forskolin-stimulated cAMP. [d]$hmGlu_2$ B_{max} = 1350 fmol/mg protein, $hmGlu_3$ B_{max} = 6100 fmol/mg protein. Agonist activity assessed as a stimulation of Ca^{2+} mobilization, antagonist activity assessed as an inhibition of glutamate-stimulated Ca^{2+} mobilization. [e]As previously disclosed (ref. 24) in two out of eight agonist format assays, low potency and submaximal (~30%) efficacy agonist responses were observed. The other six agonist format assays failed to demonstrate an agonist response above baseline. In comparison, six out of six antagonist format assays displayed consistent antagonist effects with 100% maximal inhibition of glutamate. [f]123Triaz = 1,2,3-triazol-4-yl

$hmGlu_2$ receptor cAMP and Ca^{2+} FLIPR assays:[27] Compounds **14a-g** and **16a-g** produced potent and maximally-efficacious agonist responses in cells expressing human $mGlu_2$ receptors, inhibiting forskolin-stimulated cAMP formation in $mGlu_2$-expressing cells with calculated EC_{50} values ranging from 0.58 nM (**16d**) to 74.0 nM (**16f**) (Table 2, representative concentration-response curves shown in Figure 4a). Relative to prototypic agonist **1**, $mGlu_2$ agonist potency in the current series ranged from an approximately 10-fold improvement for $C4_\beta$-substituted thiotriazoles **16c** and **16d** to a 13-fold loss in potency for **16f**. The highly potent $mGlu_2$ cAMP agonist responses observed for **14a-g** and **16a-g** are in sharp contrast to the pharmacology exhibited by thiophenylethers **9** ($mGlu_2$ antagonist IC_{50} = 7,000 nM) and **10** ($mGlu_2$ agonist EC_{50} = 1,170 nM (49% max response), antagonist IC_{50} = 15,300 nM (53% maximal response)[24] when tested under identical assay conditions. The effect of C4-stereochemistry on $mGlu_2$ cAMP agonist potency was generally modest, with EC_{50} values for diastereomeric pairs **14a**/**16a**, **14b**/**16b**, **14e**/**16e**, **14f**/**16f** and **14g**/**16g** being within 3-fold of one another. In contrast, $C4_\beta$-substituted analogs **16c** (R = CF_3) and **16d** (R = CF_2) exhibited a considerable potency enhancement (20-fold) over their $C4_\alpha$-substituted counterparts **14c** and **14d**. The remarkable increase in functional potency for these analogs may be related to a predicted decrease in pK_a of the triazole NH relative to that of unsubstituted triazole **16a** (calculated pK_a = 8.8, 5.9 and 6.8 for

16a, **16c** and **16d**, respectively).[29] Indeed, for C4$_\beta$-substituted analogs **16a-g**, a positive correlation between the calculated pK_a of the triazole NH and functional agonist potency at mGlu$_2$ (Figure 3b, r^2 = 0.85) was observed, suggesting that the deprotonated triazole may be preferred for mGlu$_2$ receptor binding. Interestingly, this relationship was not apparent in the case of either C4$_\alpha$-substituted analogs **14a-g** (Figure 3a, r^2 = 0.05) or in the combined (**14a-g, 16a-g**) dataset (r^2 < 0.35, data not shown), suggesting there may be distinct molecular drivers for the observed functional potencies between these diastereomerically-related series.

Figure 3. Relationship of calculated pK_a[a] of thiotriazole NH and functional agonist potency[b] for α-substituted thiotriazoles **14a-g** (a) and β-substituted thiotriazoles **16a-g** (b) in cells expressing recombinant human mGlu$_2$ receptors.

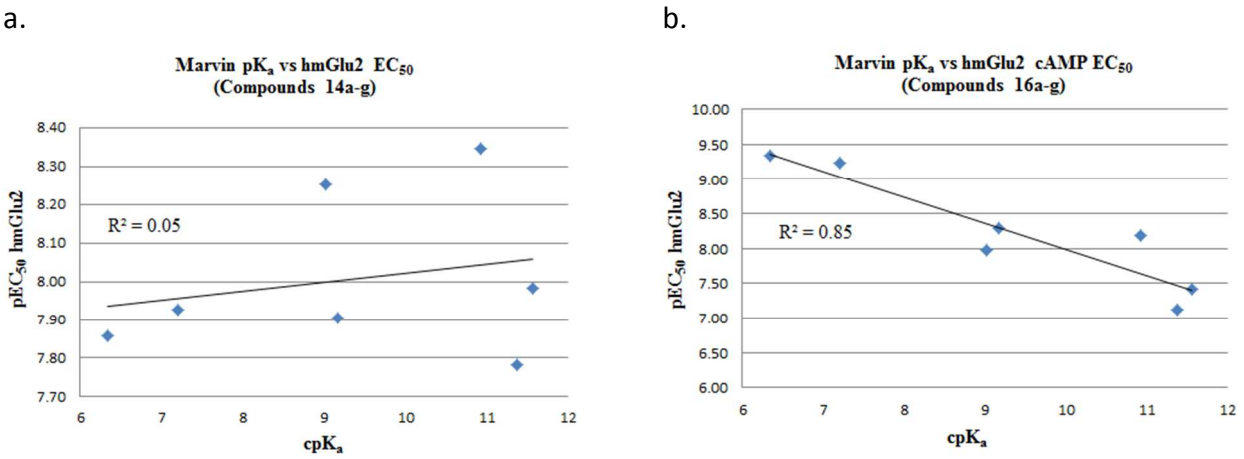

[a]Calculated values from Marvin[27]; [b]pEC_{50} values calculated from measured cAMP EC_{50} values found in Table 2. See supporting information Table S1 for the actual pK_a and pEC_{50} values used in these regression analyses.

In the hmGlu$_2$ calcium mobilization (FLIPR) assay, potent agonist responses were also generally observed across the current series (Table 2, representative compounds in Figure 4b) and highly correlated with cAMP EC_{50} values (r^2 = 0.91, supporting information Figure S2) though potencies measured in the FLIPR assay were generally lower than those derived from the cAMP format. This may be due to a number of factors associated with these two assay systems, including (a) higher receptor expression levels in cells utilized in the cAMP assay (B_{max} = 21.8 pmol/mg protein) vs. FLIPR assay (B_{max} = 1.35 pmol/mg protein), (b) less efficient coupling of hmGlu$_2$ receptors to $G_{\alpha q}$ (Ca^{2+} FLIPR) compared to $G_{i/o}$ (cAMP), (c) different experimental

conditions under which these assays are run (cAMP assay measures accumulated cAMP at 37 °C over 20 min while Ca^{2+} FLIPR measures Ca^{2+} transients at 24 °C over 2.5 min), or to some combination of these variables. The net effect of these differences leads to an overall amplification of agonist signals in the cAMP vs. Ca^{2+} FLIPR formats. Human $mGlu_2$ receptor binding affinity was highly correlated with functional agonist potency measured in both cAMP (r^2 = 0.77) and FLIPR (r^2 = 0.65) formats (supporting information Figure S3). Relative to $hmGlu_2$ binding affinity, agonist potency in the cAMP assay was left-shifted approximately 5-fold (for **16a**, **16b**, **16e**, **16f)** to 20-fold (for **14a**, **16c, 16d, 16g**). In contrast, agonist potency in the Ca^{2+} FLIPR assay was less markedly left-shifted relative to affinity, with Ki / EC_{50} ratios ranging from 1-7. The degree of agonist efficacy in the $hmGlu_2$ Ca^{2+} FLIPR assay format was generally high (80-100%) with the exception of **16f**, which showed a somewhat blunted maximal response (Emax = 71%). Compared to C4-unsubstituted analog **1** (EC_{50} = 34.4 nM), $mGlu_2$ Ca^{2+} FLIPR agonist potency for compounds in this series ranged from 4- to 5-fold improvement for **16c** and **16d** (EC_{50} = 7.8 nM and 6.3 nM respectively) to a 7-fold loss in potency for **16f** (EC_{50} = 242 nM). In contrast to thiotriazole analogs **14a-g** and **16a-g**, comparator thiophenylether analogs **9** and **10** did not produce discernible agonist responses in the $mGlu_2$ Ca^{2+} FLIPR assay.

Figures 4a-d. Representative agonist concentration-response curves for **1**, **14a**, **16a**, **16b**, **16c**, and **16f** in cells stably expressing recombinant human $mGlu_2$ and $mGlu_3$ receptors.[a]

Figure 4a. Inhibition of forskolin-stimulated cAMP production in cells expressing recombinant human $mGlu_2$ receptors by representative compounds from the current investigation

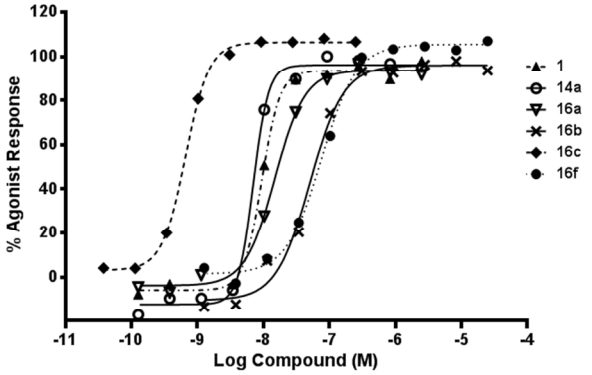

Figure 4b. Stimulation of intracellular Ca^{2+} release in cells expressing recombinant human $mGlu_2$ receptors by representative compounds from the current investigation

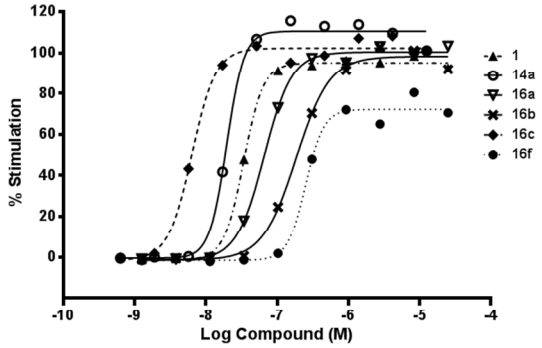

Figure 4c. Inhibition of forskolin-stimulated cAMP production in cells expressing recombinant human $mGlu_3$ receptors by representative compounds from the current investigation

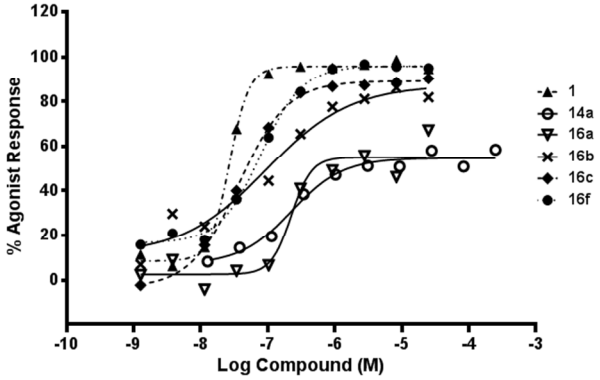

Figure 4d. Stimulation of intracellular Ca^{2+} release in cells expressing recombinant human $mGlu_3$ receptors by representative compounds from the current investigation

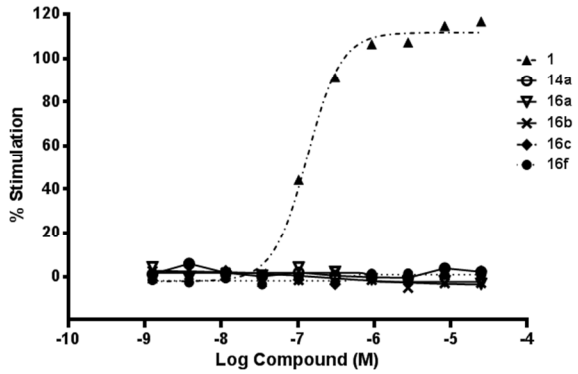

[a]See experimental section for details

hmGlu$_3$ receptor cAMP and Ca^{2+} FLIPR assays:[27] Compounds **14a-g** and **16a-g** produced agonist responses in the hmGlu$_3$ cAMP agonist assay with calculated EC$_{50}$ values ranging from 27.3 nM (**16d**) to 281 nM (**14f**) (Table 2, representative compounds in Figure 4c). As was observed for mGlu$_2$, mGlu$_3$ cAMP agonist potency correlated well with binding affinity (r^2 = 0.67, supporting information Figure S4. Relative to prototypic agonist **1** (EC$_{50}$ = 27.1 nM), mGlu$_3$ cAMP agonist activity in the current series varied from being essentially equivalent to **1** for C4$_\beta$-substituted thiotriazoles **16c** and **16d** (EC$_{50}$ values = 30.5 nM and 27.3 nM, respectively) to a 10-fold loss in agonist potency for **14f** (EC$_{50}$ = 281 nM). The consistent mGlu$_3$ cAMP agonist responses observed across compounds **14a-g** and **16a-g** are in sharp contrast to the antagonist pharmacology exhibited by thiophenylethers **9** (IC$_{50}$ = 1,070 nM) and **10** (IC$_{50}$ = 3,370 nM) in this assay.[24] The effect of C4-stereochemistry on mGlu$_3$ cAMP agonist potency was generally modest, with EC$_{50}$ values for each of the diasteriomeric pairs being within 4-fold of one another. As was observed in the case of mGlu$_2$, functional agonist potency measured in the cAMP assay format was highly correlated with calculated pKa of the thiotriazole NH for β-substituted (16a-g, r^2 = 0.67) but not α-substituted (14a-g, r^2 = 0.14) analogs (Figure 5).

Figure 5. Relationship of calculated pK$_a$[a] of thiotriazole NH and functional agonist potency[b] for α-substituted thiotriazoles **14a-g** (a) and β-substituted thiotriazoles **16a-g** (b) in cells expressing recombinant human mGlu$_3$ receptors.

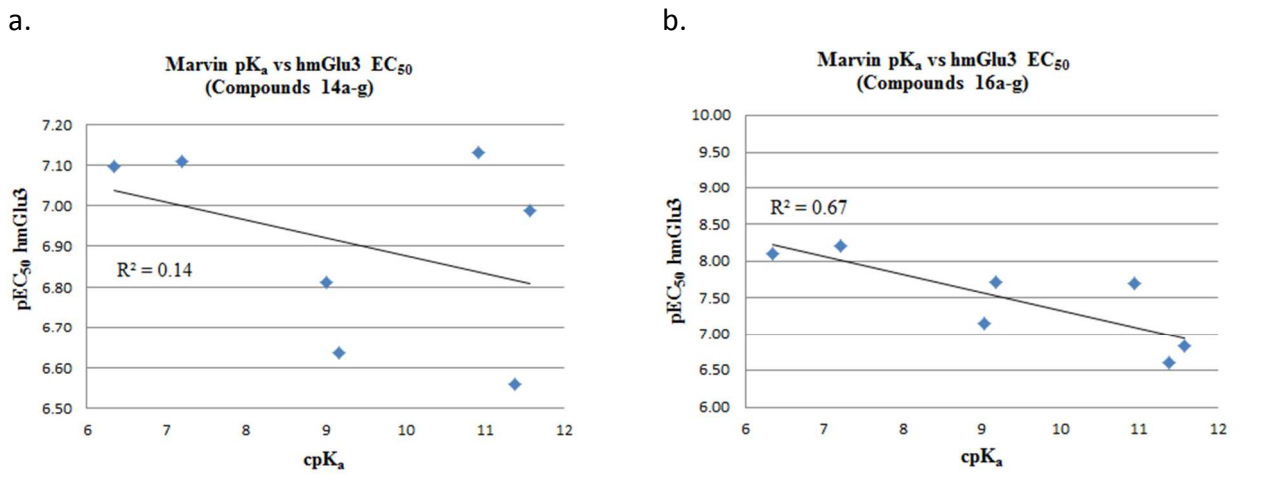

[a]Calculated values from Marvin[27]; [b]pEC$_{50}$ values calculated from measured cAMP EC$_{50}$ values found in Table 2. See supporting information Table S1 for the actual pK$_a$ and pEC$_{50}$ values used in these regression analyses.

In contrast to what was observed in the $mGlu_2$ cAMP agonist assay and in spite of the amplified agonist responses typically observed using the cAMP assay format, agonist responses in the $mGlu_3$ cAMP assay for this series were not consistently maximal (100% defined by maximal glutamate response). None of the analogs exhibited an Emax value above 90%, four (**16c**, **16d**, **16f** and **16g**) produced Emax values ≥ 80%, eight between 65-80% and two (**14a** and **16a**) elicited maximal agonist efficacies below 65% (52% and 61%, respectively). For certain compounds (**14a**, **14c**, **14d**, **14f**, **14g**, and **16a**), $mGlu_3$ cAMP antagonist IC_{50} values could be determined (Table 2, **14a** exemplified in Figure 6a), confirming the partial $mGlu_3$ agonist / antagonist characteristics of these compounds in this assay format. Functional agonist potencies in the $mGlu_3$ cAMP assay were not substantially shifted relative to $mGlu_3$ affinity, with EC_{50} and Ki values being within 3-fold of one another. The relatively small left-shift (vs. Ki) in this assay compared with that seen in the case of $hmGlu_2$ (*vide supra*) is likely the result of lower expression of $mGlu_3$ receptors in this cell line (B_{max}= 5.27 pmol/mg protein) compared to $mGlu_2$ receptor expression (B_{max}= 21.8 pmol/mg protein), resulting in lower receptor reserve.

In the $hmGlu_3$ calcium mobilization (FLIPR) assay, agonist responses (with submaximal efficacies) were observed for only two of the fourteen analogs of this series (**14b**: EC_{50} = 105 nM, E_{max} = 49% and **14c**: EC_{50} = 82 nM, Emax = 37%, Table 2). Representative concentration-response curves for members of this series are shown in Figure 4d. With the exception of **14b** and **14c**, none of the other compounds from this series produced an agonist response in this assay up to the highest concentration tested (25 μM); rather, many produced discernible though generally low potency antagonist responses. This pharmacological profile is shared by thiophenylethers **9** (IC_{50} = 7,690 nM) and **10** (IC_{50} = 6,710 nM) but is notably different when compared to the potent and maximally efficacious agonist response produced by **1** ($mGlu_3$ Ca^{2+} FLIPR EC_{50} = 140 nM, Emax = 95%). The lack of robust agonist responses for compounds in this series in the $mGlu_3$ Ca^{2+} FLIPR assay cannot be readily explained by receptor expression levels, G-protein coupling or experimental assay considerations as (a) $mGlu_3$ receptor expression levels in the Ca^{2+} FLIPR assay (B_{max} = 6.1 pmol/mg protein) are comparable to those observed in the cells used for the $mGlu_3$ cAMP assay (B_{max} = 5.27 pmol/mg protein) and higher than $mGlu_2$ levels in the $mGlu_2$ Ca^{2+} FLIPR assay (B_{max} = 1.35 pmol/mg protein) -- two assays in which consistent agonist responses were observed for these molecules; and (b) compound **1** exhibits

full agonist responses in both $mGlu_2$ and $mGlu_3$ assays, regardless of format. Rather, it appears that compounds in the current series, while binding with comparable affinity to $hmGlu_2$ and $hmGlu_3$ receptor proteins, exhibit differential functional responses at these targets, being potent and maximally (or near maximally) efficacious agonists in cells expressing $mGlu_2$ receptors and partial agonists (with varying levels of maximal effectiveness) in cells expressing $mGlu_3$ receptors. This is a pharmacological profile similar to that observed for compound **5**,[22] though with significantly enhanced $mGlu_2$ receptor potency. From this series, compound **14a** (LY2812223),[30] owing to its potent, maximally efficacious agonist effects in cells expressing $mGlu_2$ receptors and low potency and efficacy in $mGlu_3$-expressing cells (Figure 6), was selected for additional investigation.

Figure 6. Agonist and antagonist concentration-response relationship for **14a** in cells expressing recombinant human $mGlu_3$ receptors.

a. Agonist (open squares) and antagonist (closed circles) responses elicited by **14a** in $hmGlu_3$-expressing cells employing cAMP format.

b. Agonist responses elicited by **14a** in $hmGlu_2$ (closed triangles) and $hmGlu_3$ (open circles) expressing cells employing Ca^{2+} FLIPR format.

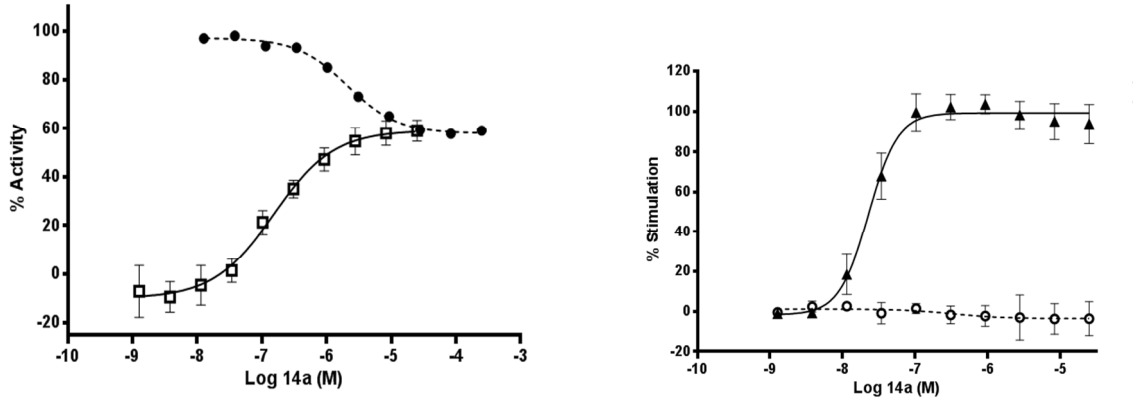

Recombinant mGluR selectivity assays.[27] Compounds **14a** was tested for its ability to elicit agonist or antagonist responses in cells expressing recombinant human mGlu receptor subtypes (Table 3). At the concentrations evaluated (25 μM for agonist, 12.5 μM for antagonist), no functional responses were observed for this molecule in cells expressing recombinant human $mGlu_1$, $mGlu_4$, $mGlu_5$ or $mGlu_7$ receptors. In contrast, agonist responses were observed for **14a** in cells expressing $hmGlu_6$ (cAMP EC_{50} = 3,450 nM, Emax = 97%)) and $hmGlu_8$ (cAMP EC_{50} =

10,100 nM, Emax = 86%). Thus, the $hmGlu_2$ agonist selectivity ratio for **14a** over $hmGlu_6$ receptors is 616 fold (based on $hmGlu_2$ cAMP EC_{50}) or, more conservatively, 163 fold (based on $hmGlu_2$ Ca^{2+} FLIPR EC_{50}), while the selectivity for **14a** over $hmGlu_8$ receptors is 1,800 fold (based on $hmGlu_2$ cAMP EC_{50}) or, more conservatively, 480 fold (based on $hmGlu_2$ Ca^{2+} FLIPR EC_{50}). In addition to its selectivity over these closely related targets, compound **14a** was evaluated against a panel of CNS receptor, transporter and ion channel targets, and against the hERG channel at a screening concentration of 10 μM. No significant effect of this molecule was observed at any of these additional targets (supporting information, Table S2).

Table 3. Functional agonist or antagonist responses of **14a** in cells expressing recombinant human mGlu receptor subtypes: EC_{50} (nM) ± SEM (Emax) or *IC_{50} (nM)* ± *SEM (Imax)*[a]

$mGlu_1$	$mGlu_4$	$mGlu_5$	$mGlu_6$	$mGlu_7$	$mGlu_8$	
Ca^{2+} FLIPR	Ca^{2+} FLIPR	Ca^{2+} FLIPR	cAMP	Ca^{2+} FLIPR	cAMP	Ca^{2+} FLIPR
>25000	>25000	>25000	3450 ± 165	>25000	10100 ± 2150	>25000
>12500	*>12500*	*>12500*	(97%)	*>12500*	(86%)	*>12500*

[a]See experimental section for methods

Molecular Modeling Studies. Previous work by our group and others has provided a detailed understanding of the binding interactions of orthosteric agonists[20a,25] and antagonists[20b] to the glutamate binding site of $mGlu_2$ and $mGlu_3$ receptors and the associated impact of ligand structure on the overall topology of the ligand-bound ATDs. Specifically, orthosteric agonists and antagonists, while binding to common hinge residues (see Table 1), stabilize distinct ATD conformations (closed for agonists, open for antagonists). Thus, with the established $mGlu_2$-agonist, $mGlu_3$ partial agonist/antagonist pharmacology of **14a** in mind, we performed modeling experiments with this molecule to the relevant crystal structures (antagonist form of $hmGlu_3$, agonist form of $hmGlu_2$) in an attempt to rationalize this unique pharmacology. Compound **14a** was built in MOE[31] directly from and superimposed onto antagonist ligand **17** (LY341495, Figure S5)[32] in the $mGlu_3$ ATD structure (3SM9)[20b] and from agonist ligand **1** in the recently

disclosed $mGlu_2$ ATD structure (4XAQ).[25] In each case, the newly built **14a** was minimized with the MMFF94x force field in MOE. No additional minimization of ligand with protein was performed to ensure no movement of ligand or residues from the original crystal structure coordinates. As can be seen in Figure 7a, modeling **14a** into the published (3SM9) antagonist-bound crystal structure of $hmGlu_3$ led to a proposed complex in which key contacts of the glutamate backbone of **14a** with lobe 1 (LB1) residues associated with the hinge domain could be readily established with no apparent steric clashes between ligand and protein. In contrast, attempts to dock **14a** into the closed, agonist-stabilized form of the $mGlu_2$ ATD derived from its complex with **1**[25] resulted in predicted severe steric clashes between the $C4_{\alpha}$-thiotriazolyl functionality and two residues, Y144 (LB1) and R271, lobe 2 (LB2) that are situated close to the C4-position of the bicyclic amino acid ring system (Figure 7b). We have previously ascribed this possible negative steric interaction as the underlying reason why relatively large (e.g. NHAc, SPh) substituents attached to this position lack agonist activity while smaller ones (e.g. F, OH, N_3, NH_2) retain this pharmacology.[24]

Figure 7. Modeling of **14a** into the antagonist bound crystal structure of $hmGlu_3$ (a) and the agonist bound crystal structure of $hmGlu_2$ (b).

a. **14a** modeled into the open (antagonist derived) form of the $hmGlu_3$ ATD (PDB: 3SM9).[20b] **14a** binding to this form of the $hmGlu_3$ ATD appears to be feasible as no close contacts between the thiotriazole substituent and the $mGlu_2$ protein are observed.

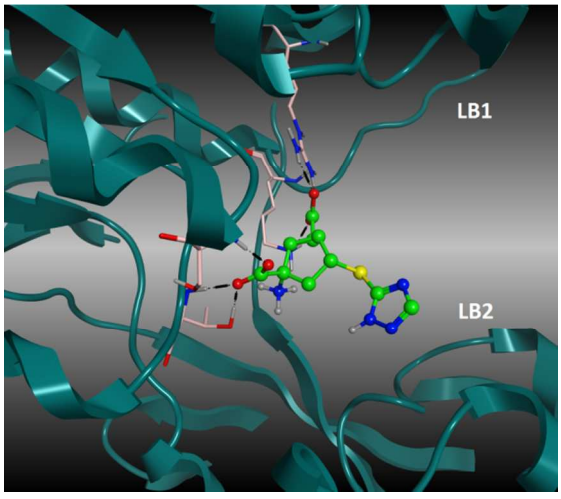

b. **14a** modeled into the closed form of the $hmGlu_2$ ATD (PDB: 4XAQ).[25] Predicted steric clashes (depicted as orange cylinders) between this structure and Y144 and R271 suggest that this molecule would not effectively bind to and stabilize the closed (agonist) state of the $hmGlu_2$ ATD.

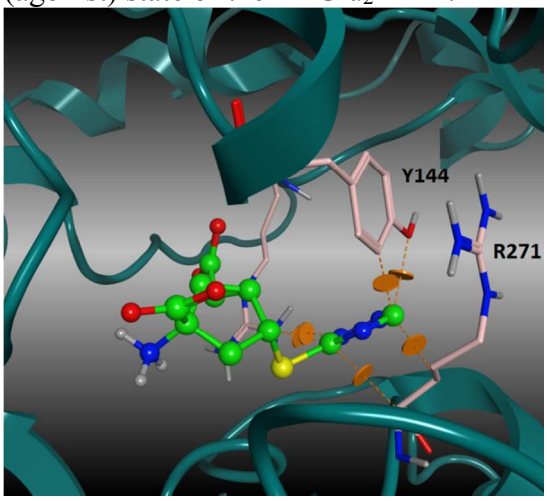

Co-crystallization studies with recombinant human $mGlu_2$ and $mGlu_3$ amino terminal domain proteins. Clearly, the predicted binding modality of **14a** to the agonist recognition site of $hmGlu_2$ ATD (Figure 7b) is incompatible with the observed potent agonist activity for this molecule in cells expressing these receptors. In an effort to understand the molecular basis for the unique pharmacological profile exhibited by **14a,** co-crystallization of this compound with the ATDs of both $hmGlu_2$ and $hmGlu_3$ was performed.[27] In the case of $hmGlu_2$, a dimeric protein was observed (supporting information, Figure S5). The following analysis pertains to protomer A for $hmGlu_2$ (as depicted in Figure S5) which possessed the highest quality electron density data. The structures of **14a** bound to the $hmGlu_2$ (2.8 Å resolution) and $hmGlu_3$ (2.9 Å resolution) ATDs are depicted in Figure 8. Inspection of the overall topology of these complexes revealed a more closed state of the $mGlu_2$-**14a** ATD complex (open angle = 27.5°, Figure 8a) compared to the $hmGlu_3$-**14a** bound structure (open angle = 45.1°, Figure 8b).[33] In each case, the α-amino acid functionality of **14a** is situated in the hinge region of the protein and involved in H-bond interactions with LB1-associated residues S165, A166 and T168 ($hmGlu_2$ numbering) while the distal (C6)-carboxylic acid of **14a** shows close interactions with LB1 residues R61 and K377 in $hmGlu_2$ (Figures 8c) and R68 in $hmGlu_3$ (Figure 8d). These interactions are identical to those we observed for co-crystals of glutamate (supporting information Figures S7, S8) and other compounds from the 2-aminobicyclo[3.1.0]hexane-2,6-dicarboxylate scaffold[25] bound to the $hmGlu_2$ and $hmGlu_3$ ATDs. In contrast, while the primary ammonium functionality of **14a** appears to form a direct H-bond interaction with lower lobe (LB2) D295 in the $mGlu_2$ complex (Figure 8c), this functionality is remote (5.5 Å) from D301 in the $mGlu_3$-**14a** structure, though possibly interacting remotely with the D301 side chain carboxylate via an intermediary water molecule (Figure 8d). In addition to these glutamate pharmacophore interactions, the $C4_\alpha$-thiotriazole group forms an H-bond interaction with LB2 residue E273 and a π-H interaction with backbone NH of S272 in the $mGlu_2$ structure (Figure 8e) while in the $mGlu_3$ complex, the thiotriazole appears to extend into the open, solvent accessible, cleft making LB1 interactions with Y150 and R64 and H-bonding through an intermediary water molecule and chloride anion to LB2 residues D221, Y222 and R277 (Figure 8f).

An overlay of $hmGlu_2$ ATD-**14a** and $hmGlu_3$ ATD-**14a** structures (protomer A in each case) was generated by aligning the atoms comprising the backbone chain (carbonyl carbon, C_α and N) of

each residue in the two crystal structures[34] and is shown in Figures 9a and 9b. Pronounced movement of LB2 relative to LB1 in the $hmGlu_2$ ATD-**14a** complex (purple) relative to that in the $hmGlu_3$ structure (gold, Figure 9a) is evident. Examined in closer detail, distinct conformational states of both the $C4_\alpha$-thiotriazole of **14a** and a LB1 tyrosine residue (Y144/150) in the $hmGlu_2$ and $hmGlu_3$ structures are apparent (Figure 9b). Comparing the **14a**-$hmGlu_2$ ATD structure with the analogous **1**-$hmGlu_2$ ATD complex 4XAQ[25] (Figure 9c) it appears that a nearly 90° rotation of the C_α-C_β bond of Y144 (Figure 10a) from its position in the previously described structure with **1**[25] occurred. This provides an expanded agonist binding pocket adjacent to the C4-position of **1** and enables the $C4_\alpha$-thiotriazole ring of **14a** to both avoid steric clashes predicted from previous agonist-bound structures (Figure 7b) and engage in productive LB2 interactions, specifically with residues S272 and E273. It is noteworthy that the latter residue is not conserved in the $mGlu_3$ receptor, where it is instead a one-carbon shortened acidic amino acid, D279. We therefore propose that the ability of **14a** to stabilize the closed form of $mGlu_2$ and produce an agonist response is due to energetically productive interactions with S272 and E273, and that this cannot be effectively achieved with $mGlu_3$ owing to the inability of the thiotriazole functionality of **14a** to reach and form stabilizing LB2 H-bond contacts with D279. Interestingly, in protomer B (see supporting information Figure S6) of the **14a**-$mGlu_2$ crystal structure similar stabilizing interactions between compound **14a** thiotriazole, S272 and E273 are evident, but the movement of Y144 is far less pronounced than in protomer A, and the overall position of this residue is comparable to that found in the crystal structure of **1** with $hmGlu_2$ (Figure 9d). Specifically, in protomer B, no apparent rotation about the C_α-C_β bond has occurred. Rather, a slight (20°) rotation about the C_β-C_{Ar} bond (Figure 10b) compared to that present in previously described structure with **1**[25] is evident. This rather subtle movement is sufficient to both minimize steric clashes with the bound ligand and allow the $C4_\alpha$-thiotriazole substituent access to the LB2 interacting residues S272 and E273, perhaps owing to this structure exhibiting a slightly more open angle of the binding cleft (28.6° vs. 27.5° found in protomer A).

Figure 8. Structure of **14a** bound to the amino terminal domains (protomer A) of human $mGlu_2$ (a, c) (residues 2-493 with C121S / C234S mutation and C-His tag, PDB ID: 5CNJ) and human $mGlu_3$ (b, d) (residues 2-507 with C240S mutation and C-His tag, PDB ID: 5CNM).[27]

a. 2.8 Å $hmGlu_2$ ATD -**14a** crystal structure. The proximity of both the upper (LB1) and lower (LB2) domains to bound ligand results in an open angle of approximately 28°.[33]

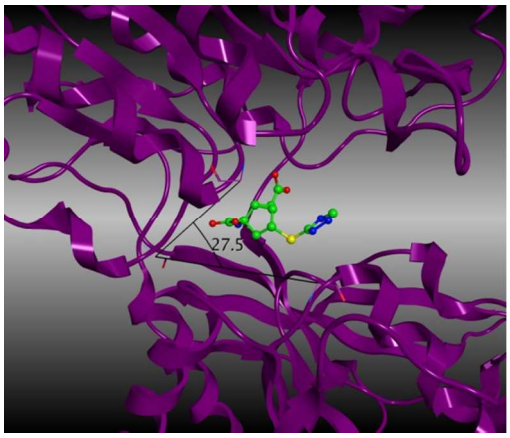

b. 2.9 Å $hmGlu_3$ ATD-**14a** crystal structure. While close association of the bound ligand with the upper (LB1) domain is evident, no direct interaction with the lower (LB2) domain with ligand is apparent, leading to an open angle of approximately 45°.[33]

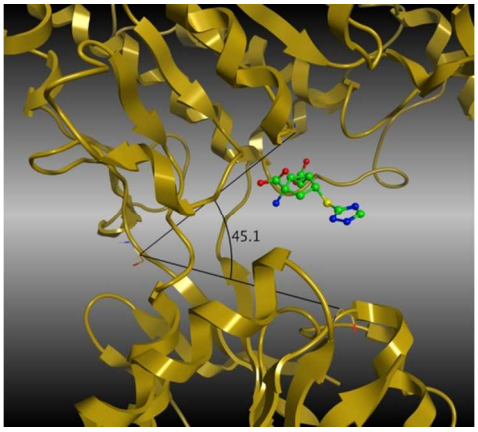

c. Site view of $hmGlu_2$ ATD-**14a** complex. Note direct interaction between C2-ammonium functionality in **14a** with side chain carboxylate of LB2 residue D295.

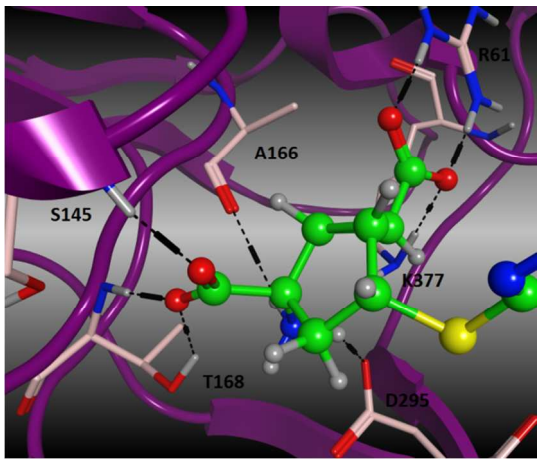

d. Site view of $hmGlu_3$ ATD-**14a** complex. The C2 ammonium functionality of **14a** is distant from LB2 residue D301 and interacts with a water molecule positioned between the ligand and D301 (not shown).

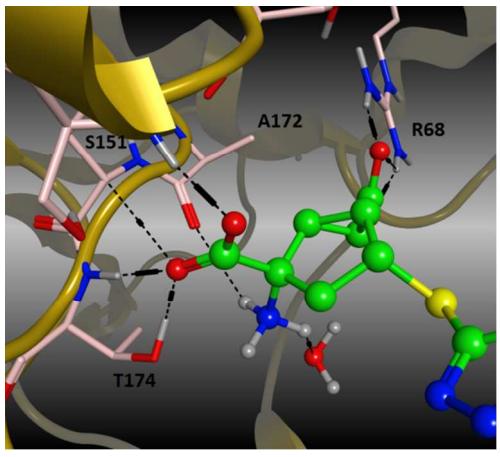

e. Site view of the C4$_\alpha$-thiotriazole interactions in the hmGlu$_2$ ATD-**14a** complex. An H-π interaction (cyan dashed line) with LB2 residue S272 and an H-bond with LB2 residue E273 is observed, which are proposed to provide additional stabilization of the closed ATD structure.

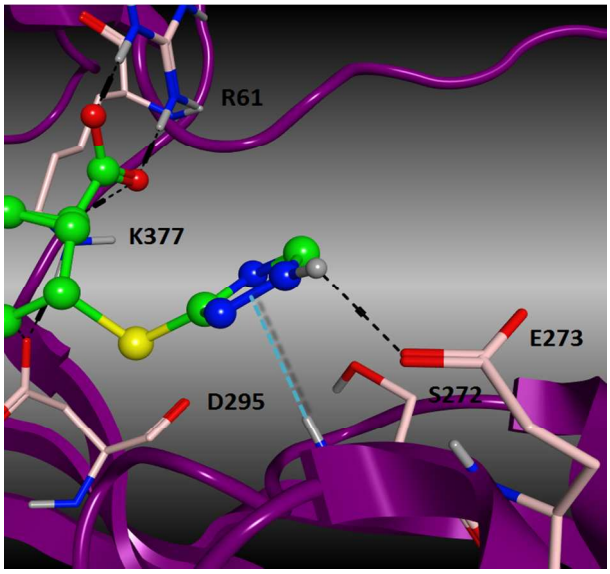

f. Site view of the C4$_\alpha$-thiotriazole interactions in the hmGlu$_3$ ATD-**14a** complex. No direct interactions with LB2 are apparent. Indirect interaction of the thiotriazole with LB2 through a water molecule and chloride ion can be observed. Indirect interactions with LB1 residue R64 and LB2 R277 may also be occurring, though no specific water molecule densities could be resolved in this region.

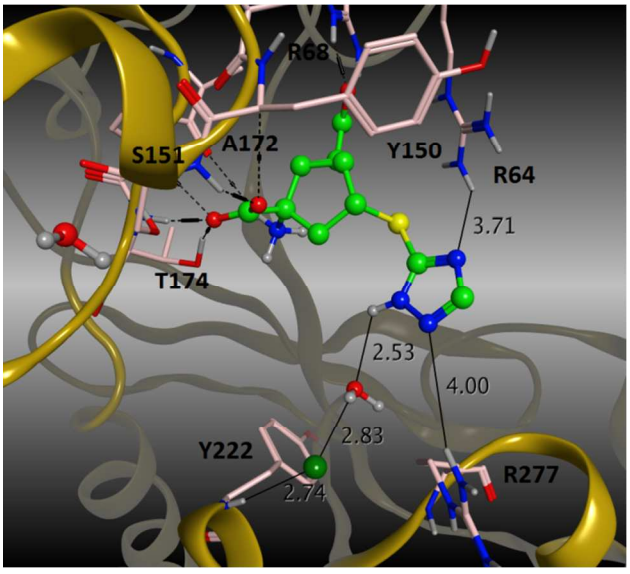

Figure 9. Overlay of protomer A crystal structures of $hmGlu_2$-**14a** and $hmGlu_3$-**14a**

a. Overlay of $hmGlu_2$ ATD-**14a** (purple) and $hmGlu_3$ ATD-**14a** (gold) structures. Fixed alignment of upper lobe (LB1) resides in the two proteins highlights the relative movement of the $hmGlu_2$ lower lobe (LB2) domain relative to that for $hmGlu_3$.

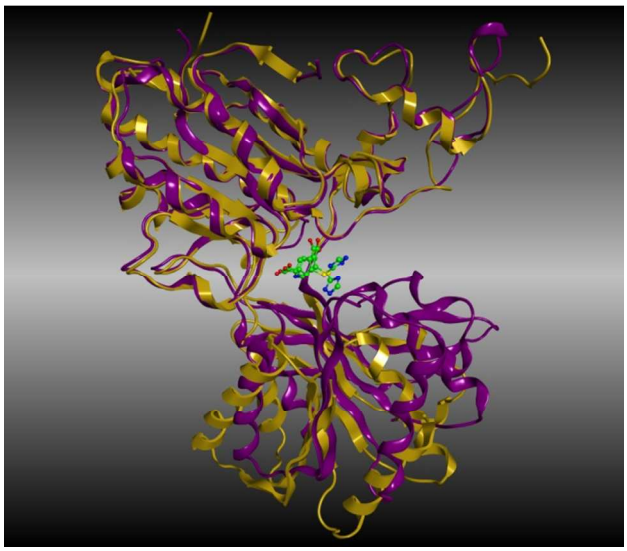

b. Detail in overlay of $hmGlu_2$ ATD-**14a** (purple protein and ligand) and $hmGlu_3$ ATD-**14a** (gold protein and ligand) structures. Note the distinct conformations of thiotriazole substituents and tyrosine residues in these structures.

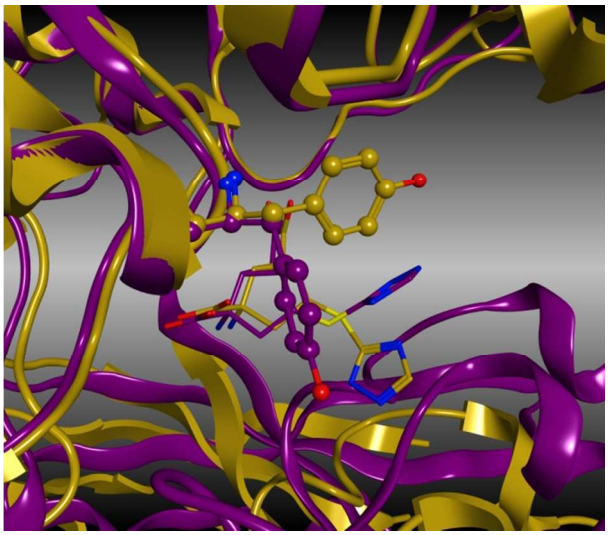

c. Overlay $hmGlu_2$-**14a** protomer A crystal structure (purple) with $hmGlu_2$-**1** crystal structure (4XAQ, cyan).[25] Note the nearly 90° rotation of Y144 from its position in structure **1**. This movement opens a large cavity into which the triazole ring of **14a** projects, allowing interaction with LB2 residues including E273.

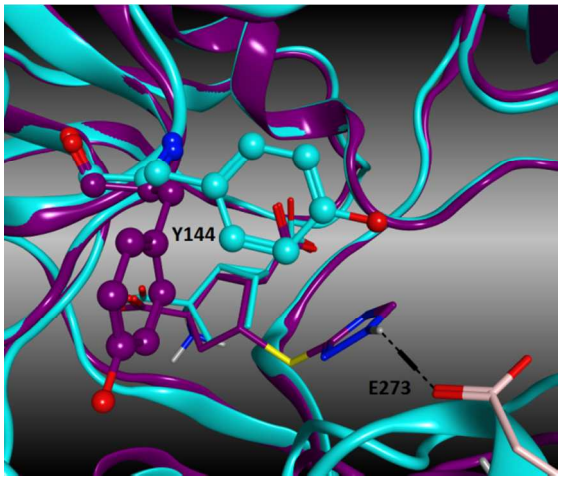

d. Overlay $hmGlu_2$-**14a** protomer B crystal structure (orange) with $hmGlu_2$-**1** crystal structure (4XAQ, cyan).[25] Note that in this protomer, Y144 adopts a similar overall conformation to that found in the $mGlu_2$-**1** structure.

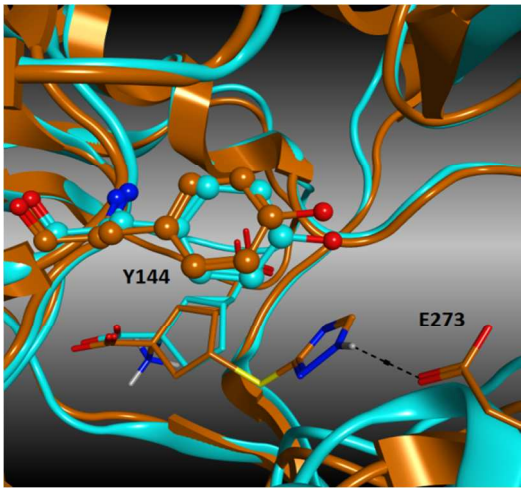

Figure 10. Y144 rotations observed in the individual $hmGlu_2$ ATD-**14a** protomer crystal structures relative to the position of this residue in the $hmGlu_2$-**1** crystal structure (PDB: 4XAQ).

a. Protomer A. 90° rotation of the Y144 Cα-Cβ bond in the $hmGlu_2$-**14a** structure (cyan) relative to the $hmGlu_2$-**1** structure (purple).

b. Protomer B. 20° rotation of the Y144 C_β-C_{Ar} bond in the $hmGlu_2$-**14a** structure (cyan) relative to the $hmGlu_2$-**1** structure (purple).

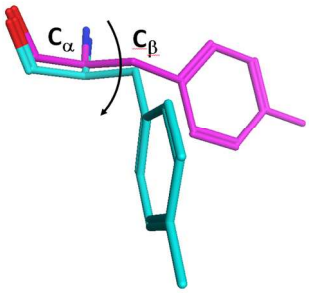

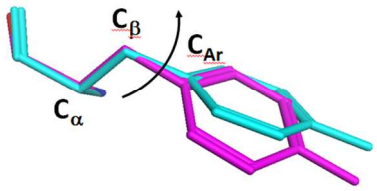

Site-Directed Mutants of $mGlu_2$ and $mGlu_3$. Given the pharmacological selectivity for **14a** for activation of $mGlu_2$ vs. $mGlu_3$ receptors and the observed close proximity of the triazole ring to $mGlu_2$ residues (E273 and L300) that are different in $mGlu_3$ (D279 and Q306), we constructed cells transiently transfected with $hmGlu_2$ wild type (WT), E273D and L300Q receptors as well as cells expressing $hmGlu_3$ WT, D279E and Q306L receptors. In these experiments, we compared the agonist responses of **14a** to glutamate (Figure 11 and Table 4) and to **18** (LY379268, Figure S5), a previously reported potent $mGlu_{2/3}$ receptor agonist[35] (data included in the supporting information section, Figure S9). Neither single (E273D, L300Q) or double (E273D + L300Q) $hmGlu_2$ mutants had any impact on the potency elicited by glutamate when compared to WT $mGlu_2$ expressing cells (Figure 11a, Table 4).[25] In contrast, the response to **14a** appears to be affected by these point mutations (Figure 11b), with agonist potency, though not maximal efficacy (100% defined as the maximal response obtained with glutamate), being slightly right-shifted in cells expressing $mGlu_2$ E273D (EC_{50} = 46.3 nM) and E273D + L300Q (EC_{50} = 48.2 nM) mutants compared to $mGlu_2$ WT receptors (EC_{50} = 20.1 nM), while maximal efficacy, but not potency, was modestly altered in the L300Q mutant. Neither potency nor efficacy of **18** was altered by either single or double mutations (Figure S4).

In comparison, cells expressing $mGlu_3$ receptor mutants D279E and D279E + Q306L, (but not Q306L alone) negatively impacted the potency of glutamate compared to cells expressing WT $mGlu_3$ receptors (EC_{50} values = 1μM, 4.2 μM and 5.1 μM, for WT, D279E and D279 + Q306L, respectively; Table 5, Figure 11c).[25] In sharp contrast, we observed a clear beneficial effect of $mGlu_3$ mutations on both agonist potency (EC_{50} values = 5.7 μM, 2.2 μM, 2.8 μM and 1.2 μM for WT, D279E, Q306L and D279 + Q306L, respectively) and maximal efficacy (Emax values = 20%, 47%, 41% and 66% for WT, D279E, Q306L and D279 + Q306L, respectively) of **14a** (Table 5, Figure 11d). These effects are also distinct from those observed for **5**, another functionally $mGlu_2$-selective agonist which appeared to gain agonist function in cells expressing the $hmGlu_3$ (Q306L) mutation, but not in the other $hmGlu_3$ mutant cell lines (D279E and combined Q306L + D279E).[25] As in the case of $mGlu_2$, neither potency nor efficacy of **18** was altered by either single or double mutations of $mGlu_3$ (Figure S9).

The observed modest loss of agonist potency of **14a** in $mGlu_2$ cells expressing the E273D mutant, combined with loss of agonist maximal efficacy in the $mGlu_2$ L300Q mutant, taken together with the reciprocal gain of agonist potency and efficacy in the $mGlu_3$ mutants (D279E, Q306L, D279E + Q306L) is in agreement with the hypothesis that these amino acids are involved in the pharmacological profile exhibited by **14a** in cells expressing WT receptors. However, it is also clear that these amino acids alone do not fully explain the observed $mGlu_2$ receptor agonist, $mGlu_3$ receptor antagonist pharmacological profile of this molecule. A limitation of this investigation should be noted. Because transient transfections result in a population of cells expressing varying levels of receptor, it was not possible to determine how, if at all, differing receptor expression levels in each transient cell line may have impacted ligand potency or efficacy. However, the fact that the potency of glutamate was unaffected in any of the $mGlu_2$ mutants vs. WT, and the potency of glutamate was only modestly (and negatively) affected in the $mGlu_3$ mutant (D279E) which led to enhance functional agonist activity for **14a** provides some evidence that any differences in receptor expression levels were not the cause of the differential effects of **14a** in these experiments. This is further supported by the lack of mutation effects on either the potency or efficacy of **18** (supporting information, Figure S9).

Table 4. Effect of L-glutamate (L-Glu) and **14a** on second messenger (Ca^{2+}, FLIPR) responses in cells transiently transfected with wild type (WT) and mutant human $mGlu_2$ receptors.[a,b]

	WT		E273D		L300Q		E273D + L300Q	
	EC_{50} ± SD (nM)	Emax ± SD (%)	EC_{50} ± SD (nM)	Emax ± SD (%)	EC_{50} ± SD (nM)	Emax ± SD (%)	EC_{50} ± SD (nM)	Emax ± SD (%)
L-Glu	1827 ± 378	94 ± 2	2351 ± 689	91 ± 4	1767 ± 518	93 ± 6	2575 ± 763	88 ± 6
14a	20.1 ± 2.3	108 ± 5	46.3 ± 8.2**	107 ± 4	22.1 ± 3.7	100 ± 3*	48.2 ± 6.2**	105 ± 5

[a]See experimental section for details; [b]Two way ANOVA followed by Dunnett's test performed in statistical analysis; *$p<0.05$ vs. $mGlu_2$ WT; **$p<0.0001$ vs $mGlu_2$ WT

Table 5. Effect of L-glutamate (L-Glu) and **14a** on second messenger (Ca^{2+}, FLIPR) responses in cells transiently transfected with wild type (WT) and mutant human $mGlu_3$ receptors.[a,b]

	WT		D279E		Q306L		D279E + Q306L	
	EC_{50} ± SD (nM)	Emax ± SD (%)	EC_{50} ± SD (nM)	Emax ± SD (%)	EC_{50} ± SD (nM)	Emax ± SD (%)	EC_{50} ± SD (nM)	Emax ± SD (%)
L-Glu	1002 ± 120	111 ± 2	4182 ± 997**	104 ± 3	1484 ± 271	105 ± 2	5118 ± 1030**	104 ± 2*
14a	5676 ± 2080	20 ± 2	2181 ± 208**	47 ± 2**	2831 ± 310#	41 ± 2**	1175 ± 253**	66 ± 1**

[a]See experimental section for details; [b]Two way ANOVA followed by Dunnett's test used in statistical analysis; *$p<0.05$ vs $mGlu_3$ WT; #$p = 0.0006$ vs. $mGlu_3$ WT; **$p<0.0001$ vs $mGlu_3$ WT

Figure 11. Effect of single and double amino acid mutations of $mGlu_2$ and $mGlu_3$ receptors on functional activity of glutamate and **14a.**

a. Agonist responses produced by L-glutamate in $hmGlu_2$ wild type and mutant receptors transiently expressed in AV12 cells.[a]

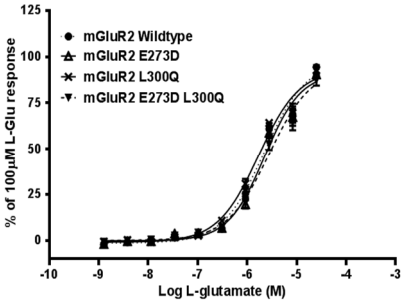

b. Agonist responses produced by compound **14a** in $hmGlu_2$ wild type and mutant receptors transiently expressed in AV12 cells.[a]

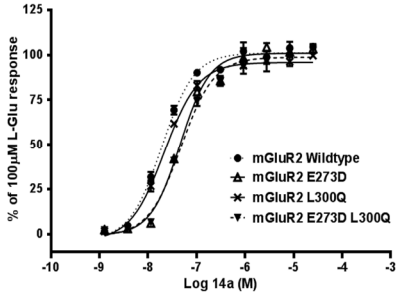

c. Agonist responses produced by L-glutamate in $hmGlu_3$ wild type and mutant receptors transiently expressed in AV12 cells.[a]

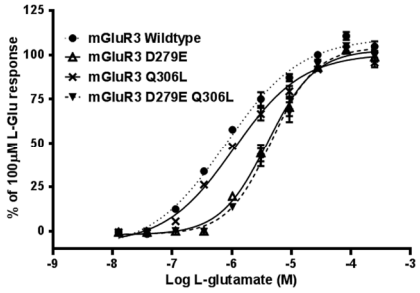

d. Agonist responses produced by compound **14a** in $hmGlu_3$ wild type and mutant receptors transiently expressed in AV12 cells.[a,b]

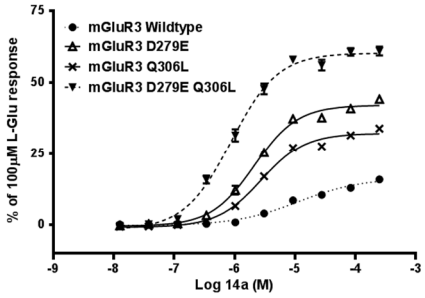

[a]See experimental section for details. [b]Note that the ordinate axis is expanded to show detail of these concentration response curves.

Pharmacokinetic Attributes of 14a. Owing to its remarkable $mGlu_2$ vs. $mGlu_3$ receptor agonist attributes and selectivity profile, **14a** was chosen for further assessment. In vitro evaluation of **14a** (Table 6) in assays that are informative regarding in vivo pharmacokinetics revealed this molecule to possess high aqueous solubility (> 100 μM at pH 7.4), no measurable microsomal metabolism across species, no significant inhibition of cytochrome P450 enzyme isoforms and high (> 98%) plasma unbound fraction.

Table 6. In vitro solubility, permeability, metabolism and protein binding of **14a**

Assay[a]	Result
Aqueous Solubility (pH 7.4)	> 100 μM
DMSO Solubility	> 10 mM
% Loss Hepatocytes (mouse, rat, dog, human)[c]	< 10% for each
% Inhibition Human Cyp Isoforms (3A4, 2D6, 2C9)[d]	< 10% for each
Plasma Unbound Fraction (rat, human)	> 98%

[a]See experimental section for methods; [b]tested at 20 μM; [c]tested at 2 μM; [d]tested at 10 μM

The in vivo pharmacokinetic attributes of **14a** were assessed in the rat, and plasma pharmacokinetic parameters are provided in Table 7. Intravenous (iv) administration of **14a** (1 mg/kg) resulted in mean peak plasma levels of approximately 9.5 μM. The rate of clearance from plasma was low (12.3 mL/min/kg) as was volume of distribution (1 L). The plasma half-life for **14a** following the 1 mg/kg iv dose was determined to be 3.3 h. Oral (po) administration of **14a** at 5 mg/kg led to relatively low plasma levels (Cmax = 0.22 μM), and an estimated oral bioavailability of approximately 4%. In contrast, intraperitoneal (ip) administration of **14a** led to dose-related increases in plasma Cmax and AUC for this compound over the range of 1-10 mg/kg with mean peak plasma concentrations being observed within 30 min of dosing and ranging from 5 μM (1 mg/kg) to 40 μM (10 mg/kg). A comparison of exposures following ip and iv dosing suggests high apparent bioavailability (73-100%) when **14a** is dosed by this route.

Table 7. Mean plasma pharmacokinetic parameters for **14a** following single intravenous, oral or intraperitoneal dosing in rats

Parameter	Units	Dose (mg/kg)				
Route		1 IV Plasma	5 PO Plasma	1 IP Plasma	3 IP Plasma	10 IP Plasma
AUC0-24hr	nM*Hours	4910 ± 934	1010 ± 60	6010 ± 754	10800 ± 7550	43100 ± 21600
Co or Cmax	nM	9540 ± 8340	220 ± 53	4920 ± 629	8050 ± 7060	31100 ± 20600
Tmax	Hours	--	0.5	0.4	0.33	0.5
CL	mL/min/kg	12.3	--	--	--	--
Vdss	L/kg	1.01	--	--	--	--
T1/2	Hours	3.3	3.7	1.2	3.2	5.2
Estimated Bioavailability	%	--	4	100	73	88

In a separate experiment, rat cerebrospinal fluid (csf) and plasma levels of **14a** were determined at 0.5h, 1h and 4h in the rat following ip doses of 1, 3, and 10 mg/kg (Figure 12, Table 8). Levels of **14a** in the csf increased proportionately with dose, resulting in mean peak csf concentrations of approximately 50 nM (1 mg/kg, 0.5h), 97 nM (3 mg/kg, 0.5h) and 272 nM (10 mg/kg, 1h). Based on the corresponding plasma levels of **14a** over this dose range and time-course, csf / plasma ratios were determined. This ratio increased linearly over time for each dose group, varying from 0.8% (0.5h, 1 mg/kg) to 3.9% (3 mg/kg, 1h, Figure 12c). Based on more conservative estimate of $hmGlu_2$ potency (Ca^{2+} FLIPR agonist EC_{50} value = 21.1 nM), the potency-normalized csf drug levels (csf concentration / EC_{50}) at 1, 3 and 10 mg/kg were found to be > 1 for all doses and time intervals with the exception of 1 mg/kg at the 4 hour time point (csf / EC_{50} ratio = 0.5). Given the high solubility, low cellular permeability and lack of protein binding for this molecule, it is proposed that cerebrospinal fluid levels are plausible estimates for the effective concentration of **14a** at extracellular $mGlu_2$ receptor binding sites in the brain.

Figure 12. Mean plasma (a) and cerebrospinal fluid (b) levels of **14a** following single intraperitoneal doses in rats[a]. (c): Time course of **14a** csf / plasma concentration ratio. Legend: 1 mg/kg (open diamonds), 3 mg/kg (closed squares), 10 mg/kg (closed triangles).

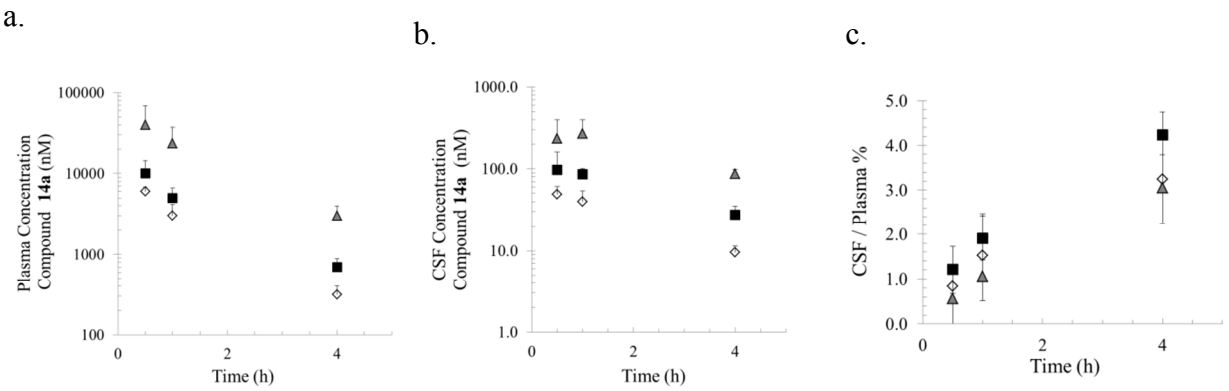

[a]See experimental section for details.

Table 8. Mean plasma and cerebrospinal fluid (csf) concentrations of **14a** following single intraperitoneal doses in rats.[a]

	Mean Plasma (nM) ± SEM			Mean csf (nM) ± SEM, [Fold over $mGlu_2$ FLIPR EC_{50}]		
Dose	0.5h	1h	4h	0.5h	1h	4h
1	6000 ± 763	3010 ± 1170	314 ± 87.9	48.8 ± 12.3 [2x]	39.9 ± 14 [2x]	9.7 ± 1.8 [0.5x]
3	10100 ± 4410	4980 ± 1650	700 ± 189	97.3 ± 63.6 [4x]	86.4 ± 15.8 [4x]	27.5 ± 7.5 [1x]
10	40100 ± 28700	23600 ± 13800	3020 ± 928	235.0 ± 160 [11x]	272 ± 126 [13x]	86.7 ± 12.5 [4x]

[a]See experimental section for details

In vivo assessment of 14a in an $mGlu_2$ receptor-dependent animal model. Given the favorable pharmacological and pharmacokinetic attributes of **14a**, the effect of this molecule on phencyclidine (PCP) evoked ambulations in rats, an animal model of psychosis known to be sensitive to $mGlu_2$-receptor (and not to $mGlu_3$-receptor) activation[12] was evaluated (Figure 13a). Intraperitoneal administration of **14a** (1 - 30 mg/kg) 30 min prior to PCP (5 mg/kg, s.c.), produced a dose-related decrease in horizontal ambulations (measured over 60 minutes immediately following PCP dosing), resulting in a calculated ED_{50} of 1.2 mg/kg (Figure 13a). In order to rule out potentially confounding effects of non-specific motor impairment in this assay, **14a** was evaluated in rats using the rotarod test (Figure 13b).[27] A statistically significant impairment of neuromuscular coordination was observed 1h following a 10 mg/kg, ip dose of **14a**, but not at later time points for this dose. No impairment of rotarod performance was seen following an ip dose of 3 mg/kg. Therefore, efficacious doses of 1 and 3 mg/kg **14a** in the PCP assay, doses that afford csf concentrations of **14a** under 90 nM (2-fold and 4-fold over its EC_{50} value at $mGlu_2$ receptors, respectively; Table 7) are not confounded by non-specific motor effects, while a transient impairment of motor function occurred at a time point corresponding to csf levels approaching 300 nM (13-fold over the $mGlu_2$ receptor EC_{50} value).

Figure 13. Behavioral responses elicited by **14a** administered by the ip route in rats

13a. Dose response for **14a** in the rat PCP locomotor activation assay

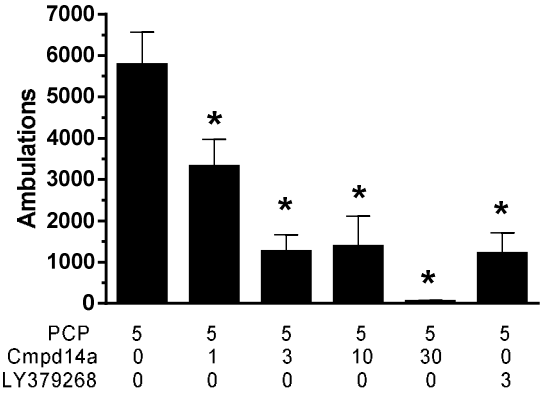

* statistically significant ($p<0.05$, ANOVA followed by Dunnett's test) compared to rats treated with PCP alone.

13b. Effect of **14a** on rotarod performance in rats

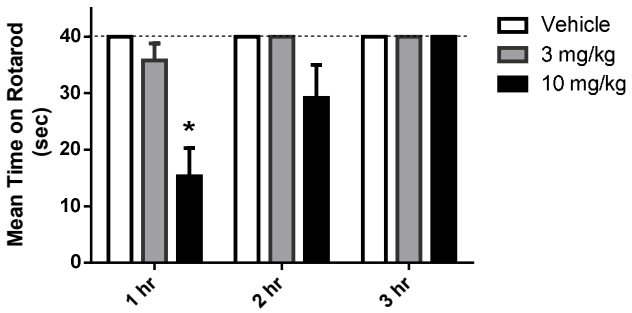

* statistically significant ($p< 0.05$) compared to Vehicle group at 1 hr.

Discussion

The therapeutic promise associated with compounds that are capable of safely modulating glutamate neurotransmission has continued to drive interest in identifying potent and selective modulators of metabotropic glutamate receptors 2 and 3, as these targets have shown great potential for the treatment of both psychiatric and neurological disorders. To this end, we have continued our investigation of substitution of the C4-position of **1**, a highly potent agonist acting at both $mGlu_2$ and $mGlu_3$ receptors. Prior work focused on this position of the bicyclohexane ring system had revealed remarkable pharmacological breadth, including the identification of sub-nanomolar potency $mGlu_{2/3}$ agonists (e.g. **7**), low potency $mGlu_{2/3}$ antagonists (e.g. **9**, **10**) and a single example of a molecule (**5**) possessing $mGlu_2$ agonist / $mGlu_3$ antagonist pharmacology. In the present investigation, we have detailed the SAR pertaining to $C4_\alpha$- and $C4_\beta$-substituted thiotriazolyl-substituted bicyclohexane amino acids related to **1**, an effort that has resulted in multiple highly potent and maximally efficacious $mGlu_2$ receptor agonists. Each of the new analogs prepared displayed $mGlu_2$ cAMP EC_{50} values under 100 nM (and Emax values > 95%), with two (**16c** and **16d**) exhibiting agonist potencies under 1 nM. Similarly, when assessed in cells co-expressing $hmGlu_2$ and the promiscuous G-protein ($G_{\alpha q}$), a system that does not produce the same degree of signal amplification as observed in the cAMP assay, each of the compounds from the current investigation maintained high potency (EC_{50} values < 100 nM for 12 of 14 analogs) and efficacy (Emax values > 80% for 13 of 14 compounds). Binding affinity and functional agonist potency for $mGlu_2$ were highly correlated, regardless of assay format. Based on these collective findings, we conclude that **14a-g** and **16a-g** are potent, highly efficacious $mGlu_2$ receptor agonists. Notably, the effects of compounds from the current investigation at $mGlu_3$ receptors were distinct from those observed against $mGlu_2$. While $mGlu_3$ receptor affinity was well-correlated with cAMP agonist functional potency, submaximal efficacy in this amplified assay format was generally observed, and when assessed in the Ca^{2+} FLIPR assay format, nearly all (12 out of 14) compounds lacked a discernable $mGlu_3$ agonist response when tested at concentrations up to 25 μM. Instead, $mGlu_3$ antagonist pharmacology was generally observed for this series. This in vitro profile is not only distinct from prior, pharmacologically mixed $mGlu_{2/3}$ receptor agonists (e.g. **1, 2, 7, 8** and **18**),[5,6,24,25,35] but also from

compound **5**, as this $C4_{\alpha}$-methyl substituted variant does not elicit an agonist response even when assessed in the amplified $mGlu_3$ cAMP agonist assay.[22] Within the context of the current SAR, an intriguing relationship between the calculated pKa of the thiotriazole NH and both $mGlu_2$ and $mGlu_3$ functional agonist potency for $C4_{\beta}$-, but not $C4_{\alpha}$-substituted analogs was revealed. This diastereoselective effect of triazole pKa on agonist potency suggests that even within this series of functionally selective Glu2 receptor agonists, distinct binding interactions for the $C4_{\alpha}$- and $C4_{\beta}$- subseries with $mGlu_{2/3}$ receptors may be involved, though modeling experiments have not yet provided a clear understanding for this finding. In an effort to better understand the molecular basis for the observed pharmacology for **14a**, moderately resolved co-crystal structures with the $hmGlu_2$ and $hmGlu_3$ ATDs were obtained. In agreement with the hypothesis that agonists stabilize a closed, and antagonists an open, conformation of the ATD, compound **14a** was found to co-crystallize with the closed form the $mGlu_2$ ATD (protomer A open angle = 27.5°) and the open form of $mGlu_3$ (protomer A open angle = 45.1°). The $mGlu_2$ open angle found with agonist **14a** is similar, though slightly greater (approximately 3°) than those observed for other agonists co-crystallized with either $mGlu_2$ (glutamate, 24.7°; **1**, 4XAQ, 24.7°; **8**, 4XAS, 24.2°) or $mGlu_3$ (glutamate, 24.8°; **1**, 4XAR, 24.8°), while the $mGlu_3$ open angle observed with **14a** is comparable, though slightly (approximately 2.4°) more open than that measured for the published $mGlu_3$ structure (3SM9)[20b] in complex with antagonist ligand **17** (42.7°). While at first glance the $mGlu_3$-**14a** co-crystal structure suggests the thiotriazole substituent of **14a** is not involved in specific protein interactions, closer inspection revealed an ordered ligand-protein complex in which the triazole is in fact directly interacting with LB1 residue R64 (and perhaps Y144) and indirectly with LB2 domain residues Y222 (via a water molecule and chloride ion) and possibly R271 via a proposed water molecule which is certainly present in this solvent-exposed space, though not resolved in the crystal structure. In the $mGlu_2$-**14a** structure, it appears that either a large (in protomer A) or subtle (in protomer B) movement of LB1 residue Y144 allows for the direct and productive interaction of the thiotriazole substituent of **14a** with two LB2 residues, S272 NH with the triazole π-system and E273 carboxylate with (presumably) the triazole NH. We propose that these energetically favorable **14a**-LB2 interactions in the $mGlu_2$ receptor provide sufficient stabilization of the overall closed ligand-protein complex to enable agonist signaling, while weaker stabilization of a closed ATD-**14a** structure is predicted in the case of $mGlu_3$ owing to the presence of the one-atom shortened

acidic amino acid residue (D279) in place of the E273 found in $mGlu_2$. In partial support of this hypothesis, site directed mutagenesis experiments in which $mGlu_2$ glutamate residue E273 was replaced with an aspartate resulted in a reduction of agonist potency, though not maximal efficacy for **14a**, while the reciprocal mutation of $mGlu_3$ aspartate residue D279 with a glutamate led to a gain in both **14a** agonist potency and efficacy. As part of this site-directed mutagenesis study, we also generated an $mGlu_3$ mutant in which glutamine residue Q306 was replaced with a leucine. This mutation (and its reciprocal $mGlu_2$ L300Q) was found to play a role in the observed $mGlu_2$ agonist, $mGlu_3$ antagonist pharmacology of compound **5**.[25] Interestingly, we found an enhanced agonist response of **14a**, similar to that seen in the D279E mutant, when examined in the $mGlu_3$ Q306L cells. Furthermore, a combination of these mutations ($mGlu_3$ D279E + L300Q) resulted in a further gain of agonist potency and efficacy, suggesting that these residues collectively influence agonist responses observed for **14a**. On the other hand, the $mGlu_2$ double mutant (E273D + L300Q) did not result in a diminished agonist response for **14a** compared to that seen in the E273D mutant alone. Hence, while these residues are likely playing some role in the observed pharmacological profile of **14a**, it is clear that they alone cannot account for the potency and efficacy measured for this molecule in WT receptors. The potency (EC_{50} 1,175 nM) and efficacy (Emax = 66%) of **14a** observed in the $mGlu_3$ D279E + Q306L cells is considerably lower than that observed in WT $mGlu_2$ receptors (EC_{50} = 20 nM, Emax = 108%). Likewise, the very weak agonist potency and efficacy of **14a** in WT $mGlu_3$ receptors (EC_{50} = 5,676 nM, Emax = 20%) was not recapitulated in the $mGlu_2$ E273D mutant construct (EC_{50} = 46.3 nM, 107%).

Finally, owing to its interesting pharmacological profile compound **14a** was chosen for additional profiling. As has been generally observed for other members of this chemotype, **14a** showed excellent selectivity when evaluated against the other mGlu receptor subtypes, with only weak agonist responses observed at two other mGlu receptor subtypes, $mGlu_6$ (EC_{50} = 3450 nM) and $mGlu_8$ (EC_{50} = 10,100 nM). Furthermore, when examined against a broader array of biological targets (receptors, enzymes, ion channels), no substantial effects were observed at the screening concentration (typically 10 μM). Consistent with other compounds of this chemical series, **14a** was found to possess high aqueous solubility and plasma unbound fraction and low passive permeability, hepatocyte metabolism, and cytochrome P450 inhibition. When administered to rats by the iv route, **14a** displayed both low clearance and volume of distribution,

consistent with this molecule being restricted to the extracellular compartment. As expected for a highly polar, charged amino diacid, **14a** showed poor oral bioavailability, but when dosed by the ip route, rapid access to plasma was observed (Tmax within 30 min) and plasma concentrations were dose-proportionate over the 1-10 mg/kg range (dose vs Cmax: $r^2 = 0.99$; dose vs. AUC: $r^2 = 0.99$, data not shown). Drug levels in the csf were observed at the earliest assessed time-point (30 min), were low (approximately 1-4%) compared to plasma levels, and increased with both dose and time interval over 4h. Interestingly, the csf / plasma ratio appeared to increase over time, suggesting a slower rate of clearance of **14a** from the central compartment relative to plasma. Over the investigated dose range, csf levels exceeded the $mGlu_2$ cAMP EC_{50} value (~ 5 nM) for each dose and time point up to 4 h post dose, and exceeded the $mGlu_2$ Ca^{2+} FLIPR EC_{50} value (~20 nM) for all doses and time intervals with the exception of 1 mg/kg at the 4 h time point. Given that **14a** has very low protein binding and does not penetrate effectively into cells, we posited that csf drug levels would be a reasonable estimate for drug concentrations at central extracellular $mGlu_{2/3}$ receptor binding sites. Consistent with this hypothesis, **14a**, (1 - 30 mg/kg, ip) showed robust efficacy in an $mGlu_2$-driven behavioral test, the reduction of PCP-evoked ambulations, with all doses producing statistically significant effects. While the effect of **14a** in this assay at 10 and 30 mg doses could be interpreted to be due to altered neuromuscular coordination (as observed in the rotarod test), the lack of functional rotarod impairment at the 3 mg/kg dose suggests that behavioral efficacy observed below 10 mg/kg in this assay was not confounded by non-specific motor effects. From a csf exposure standpoint, motor impairment does not appear to be evident for csf concentrations of **14a** below 100 nM, levels that are under 5x the $mGlu_2$ Ca^{2+} FLIPR EC_{50}. Conversely, motor impairment was at least transiently observed when csf levels reached ~250 nM, though care should be taken in interpreting these findings as csf drug levels and behavioral assessments were not performed in the same rats or study. Additional work will be needed to more fully establish the pharmacokinetic-pharmacodynamic relationship for **14a** in preclinical rodent efficacy and side effect models.

Conclusion

The current investigation has led to the identification of compound **14a**, a highly potent and efficacious agonist at $mGlu_2$ receptors that exhibits either partial agonist (cAMP assay format) or

weak antagonist (Ca^{2+} FLIPR assay format) activity at $mGlu_3$ receptors. Further characterization of **14a** has established favorable pharmacokinetic behavior in rats which translated into potent efficacy in an animal model of psychosis. Additional in vivo characterization of this molecule and an orally bioavailable prodrug form of it will be disclosed in due course. Owing to moderate resolution $hmGlu_2$ and $hmGlu_3$ co-crystal structures with **14a**, detailed insights into specific protein-ligand interactions have been revealed. These, in turn, have led to additional insights regarding the molecular interactions underpinning the functional $mGlu_2$ agonist selectivity for this molecule which may be useful in future ligand design.

Experimental Section

Synthesis. ^{1}H- and ^{13}C-NMR spectra were obtained on a Varian Unity INOVA 400 at 400 MHz and 125 MHz respectively, unless noted otherwise. TMS was used as an internal standard. LCMS data were obtained using an Agilent 1100 Series HPLC on a Gemini-NX C18 110A, 50 X 2.00 mm column. HRMS were obtained using an Agilent 1100 Series LC and TOF mass spectrometer, on a Gemini-NX C18 110A, 50 X 2.00 mm column. Optical rotations were obtained on a Perkin Elmer Polarimeter 341. Melting points were obtained on a Laboratory Devices Mel-Temp® 3.0. Microwave reactions were run in a Biotage Initiator Microwave. Capillary Electrophoresis was performed on a Agilent Technologies 3D-CE equipped with a deuterium lamp, a photodiode array detector, and a 50 mm i.d., 363 mm o.d. fused-silica capillary, Ld: 40 cm, Lt: 48.5 cm. Separations were conducted at 20 ^{0}C at a voltage of 25 kV. Reactions were monitored by thin layer chromatography using silica gel 60 F_{254} plates from EMD and staining with ninhydrin. Unless otherwise noted normal phase purifications were performed using RediSep® pre-packed columns from Teledyne Isco. Cation exchange chromatography was performed using Dowex 50W X8; 50-100 mesh, which was purchased from Aldrich. On the basis of capillary electrophoresis all final compounds were >95% pure. Numbering convention used in NMR assignments is provided in Figure 14.

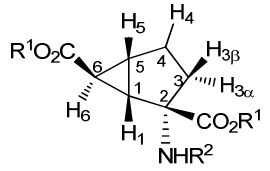

Figure 14. Numbering convention used in NMR peak assignments.

General Procedure A: Preparation of C4 thiotriazoles 13a-g, 14a-g. A mixture of tosylate **11** (1.00 equiv.) or bromide **12** (1.00 equiv.), 5-substitued-4*H*-1,2,4-triazole-3-thiol (1.3-1.9 equiv.), and sodium or potassium carbonate (1.5-2.0 equiv.) in dimethylformamide (0.2 M) was heated to 70-80 °C for 3 hours in a microwave or overnight with conventional heating. The reaction was diluted with ethyl acetate and washed with 1 M $NaHSO_4$ (or 1 M citric acid) and brine. The organic was dried over Na_2SO_4, filtered, and concentrated in vacuo. The crude material was purified on a silica gel column eluting with a suitable organic solvent (e.g. hexanes/acetone, hexanes/ethyl acetate).

General Procedure B: Purification using Dowex cation exchange chromatography. The Dowex resin was prepared by first washing in a fritted funnel with water, THF, and water. The resin was soaked in 3N NH_4OH for 5 min then the solvent was removed by filtration. This soaking in NH_4OH was repeated. The resin was washed with H_2O until pH = 7 was achieved. Next the resin was soaked in 1N HCl for 5 min then the solvent was removed by filtration. This HCl soaking was also repeated. The resin was washed with H_2O until pH = 7 was reached. The freshly prepared resin was added to a glass column. Approximate resin bed was 1" diameter x 3" high. The crude material was dissolved in 4 mL H_2O and adjust to pH = 4. The material was carefully loaded to the top of the resin bed. The eluent drip rate was maintained at 1 drop every 2-3 seconds. After initial loading volume dropped to the resin surface, 5 mL H_2O was added. After the solvent dropped to the resin bed the column was filled with water and the drip rate maintained. The pH of the eluent was closely monitored. Once the pH dropped to 0 then returned to pH = 7 the flow rate was increased. The column was washed with 5 column volumes of water, 10 column volumes of 1/1 H_2O /THF, then 10 column volumes H_2O. All eluent up to this point was discarded. The compound was displaced from the resin by washing with 15 column volumes of 10% aq. pyridine.

Di-*tert*-butyl (1*R*,2*S*,4*R*,5*R*,6*R*)-2-(*tert*-butoxycarbonylamino)-4-(4*H*-1,2,4-triazol-3-ylsulfanyl)bicyclo[3.1.0]hexane-2,6-dicarboxylate (13a). Following General Procedure A using **11** (708 mg, 1.25 mmol, 1 equiv.), 1*H*-1,2,4-triazole-3-thiol (169 mg, 1.62 mmol, 1.30 equiv.) potassium carbonate (345 mg, 2.49 mmol, 2.0 equiv.) and DMF (5.0 mL) the title compound, **13a** (433 mg, 0.87 mmol), was obtained in 70% yield. MS (ES+) 497.2 $[M+H]^+$. ^1H NMR (400 MHz, $CDCl_3$, δ): 12.5 (bs, 1H), 8.25 (s, 1H), 5.39 (s, 1H), 4.51 (m, 1H), 3.15 (m, 1H), 2.33 (m, 1H), 2.21 (m, 1H), 1.86 (m, 1H), 1.46 (s, 9H), 1.42 (s, 18H), 1.31 (dd, J = 14, 11 Hz, 1H).

Di-*tert*-butyl (1*R*,2*S*,4*R*,5*R*,6*R*)-2-(*tert*-butoxycarbonylamino)-4-[(5-methyl-4*H*-1,2,4-triazol-3-yl)sulfanyl]bicyclo[3.1.0]hexane-2,6-dicarboxylate (13b). Following General Procedure A using **11** (227 mg, 0.400 mmol, 1 equiv.), 5-methyl-4*H*-1,2,4-triazole-3-thiol (71.0 mg, 0.598 mmol, 1.5 equiv.) potassium carbonate (84 mg, 0.60 mmol, 1.5 equiv.) and DMF (2.0 mL) the title compound, **13b** (80 mg, 0.17 mmol), was obtained in 42% yield. MS (ES+) 511.0 $[M+H]^+$. ^1H NMR (400 MHz, $CDCl_3$, δ): 11.4 (bs, 1H), 8.01 (s, 1H), 5.27 (bs, 1H), 4.43 (m, 1H), 3.07 (bm, 1H), 2.44 (s, 3H), 2.34 (m, 1H), 2.19 (dd, J = 6.0, 3.0 Hz, 1H), 1.82 (m, 1H), 1.46 (s, 9H), 1.42 (s, 18H), 1.29 (dd, J = 14, 10 Hz, 1H).

Di-*tert*-butyl (1*R*,2*S*,4*R*,5*R*,6*R*)-2-(*tert*-butoxycarbonylamino)-4-[[5-(trifluoromethyl)-4*H*-1,2,4-triazol-3-yl]sulfanyl]bicyclo[3.1.0]hexane-2,6-dicarboxylate (13c). Following General Procedure A using **11** (11.8 g, 20.8 mmol, 1 equiv.), sodium 5-(trifluoromethyl)-4*H*-1,2,4-triazole-3-thiolate (7.70 g, 38.6 mmol, 1.9 equiv.), and DMF (100 mL) the title compound, **13c** (11.0 g, 19.4 mmol), was obtained in 94% yield. Note that no potassium carbonate was used in this example because the sodium thiolate was used instead of the thiol. MS (ES+) 587.2 $[M+Na]^+$. ^1H NMR (400 MHz, $CDCl_3$, δ): 11.7 (bs, 1H), 5.36 (s, 1H), 4.57 (m, 1H), 3.10 (bm, 1H), 2.38 (m, 1H), 2.27 (m, 1H), 1.88 (m, 1H), 1.50 (s, 9H), 1.44 (s, 18H), 1.35 (m, 1H).

Di-*tert*-butyl (1*R*,2*S*,4*R*,5*R*,6*R*)-2-(*tert*-butoxycarbonylamino)-4-[[5-(difluoromethyl)-4*H*-1,2,4-triazol-3-yl]sulfanyl]bicyclo[3.1.0]hexane-2,6-dicarboxylate (13d). Following General Procedure A using **11** (530 mg, 0.933 mmol, 1 equiv.), sodium 5-(difluoromethyl)-4*H*-1,2,4-triazole-3-thiolate (290 mg, 1.49 mmol, 1.6 equiv.), and DMF (2.8 mL) the title compound, **13d** (360 mg, 0.66 mmol), was obtained in 70% yield. Note that no potassium carbonate was used in

this example because the sodium thiolate was used instead of the thiol. MS (ES+) 569 $[M+Na]^+$. ^1H NMR (400 MHz, $CDCl_3$, δ): 6.80 (t, J = 53 Hz, 1H), 5.33 (bs, 1H), 4.54 (m, 1H), 3.12 (bm, 1H), 2.36 (m, 1H), 2.25 (m, 1H), 1.87 (t, J = 3.0 Hz, 1H), 1.49 (s, 9H), 1.42 (s, 18H), 1.34 (dd, J = 14, 10 Hz, 1H).

Di-*tert*-butyl (1*R*,2*S*,4*R*,5*R*,6*R*)-4-[(5-amino-1*H*-1,2,4-triazol-3-yl)sulfanyl]-2-(*tert*-butoxycarbonylamino)bicyclo[3.1.0]hexane-2,6-dicarboxylate (13e). Following General Procedure A using **11** (600 mg, 1.06 mmol, 1 equiv.), 5-amino-4*H*-1,2,4-triazole-3-thiolate (184 mg, 1.58 mmol, 1.5 equiv.), sodium carbonate (168 mg, 1.58 mmol, 1.5 equiv.), and DMF (6.0 mL) the title compound, **13e** (384 mg, 0.750 mmol), was obtained in 71% yield. MS (ES+) 512 $[M+H]^+$. ^1H NMR (400 MHz, $CDCl_3$, δ): 10.9 (bs, 1H), 5.37 (s, 1H), 4.95 (bs, 2H), 4.43 (m, 1H), 3.16 (bm, 1H), 2.28 (m, 1H), 2.18 (m, 1H), 1.90 (m, 1H), 1.47 (s, 9H), 1.45 (s, 9H), 1.43 (s, 9H), 1.29 (dd, J = 14, 9.8 Hz, 1H).

Di-*tert*-butyl (1*R*,2*S*,4*R*,5*R*,6*R*)-2-(*tert*-butoxycarbonylamino)-4-[(5-isopropyl-4*H*-1,2,4-triazol-3-yl)sulfanyl]bicyclo[3.1.0]hexane-2,6-dicarboxylate (13f). Following General Procedure A using **11** (252 mg, 0.444 mmol, 1 equiv.), 5-isopropyl-4*H*-1,2,4-triazole-3-thiolate (95.0 mg, 0.663 mmol, 1.5 equiv.), potassium carbonate (93 mg, 0.67 mmol, 1.5 equiv.), and DMF (2.0 mL) the title compound, **13f** (203 mg, 0.377 mmol), was obtained in 85% yield. MS (ES+) 539 $[M+H]^+$. ^1H NMR (400 MHz, $CDCl_3$, δ): 10.8 (bs, 1H), 5.25 (bs, 1H), 4.46 (m, 1H), 3.08 (sept., J = 7.1 Hz, 1H), 3.07 (bm, 1H), 2.36 (m, 1H), 2.21 (dd, J = 6.1, 2.8 Hz, 1H), 1.84 (t, J = 2.7 Hz, 1H), 1.47 (s, 9H), 1.42 (s, 18H), 1.34 (d, J = 7.1 Hz, 6H), 1.32 (m, 1H).

Di-*tert*-butyl (1*R*,2*S*,4*R*,5*R*,6*R*)-2-(*tert*-butoxycarbonylamino)-4-(1*H*-triazol-5-ylsulfanyl)bicyclo[3.1.0]hexane-2,6-dicarboxylate (13g). Following General Procedure A using **11** (5.00 g, 8.81 mmol, 1 equiv.), sodium 1*H*-1,2,3-triazole-5-thiolate dehydrate (1.52 g, 12.3 mmol, 1.4 equiv.), and DMF (40 mL) the title compound, **13g** (4.00 g, 8.05 mmol), was obtained in 91% yield. Note that no potassium carbonate was used in this example because the sodium thiolate was used instead of the thiol. MS (ES+) 497 $[M+H]^+$. ^1H NMR (400 MHz, $CDCl_3$, δ): 12.1 (bs, 1H), 7.67 (s, 1H), 5.27 (bs, 1H), 4.13 (m, 1H), 3.01 (bm, 1H), 2.18 (m, 2H), 1.79 (m, 1H), 1.46 (s, 9H), 1.45 (s, 9H), 1.44 (s, 9H), 1.30 (dd, J = 13, 10 Hz, 1H).

(1*R*,2*S*,4*R*,5*R*,6*R*)-2-Amino-4-(1*H*-1,2,4-triazol-3-ylsulfanyl)bicyclo[3.1.0]hexane-2,6-dicarboxylic acid (14a). Fully protected amino acid **13a** (433 mg, 0.872 mmol) was dissolved in 1,4-dioxane (7.0 mL) and treated with 4 M HCl in 1,4-dioxane (7.0 mL, 28 mmol, 32 equiv.) The reaction was stirred overnight at 50 °C. After cooling to rt the mixture was concentrated in vacuo and purified via cation exchange following **General Procedure B**. The eluent containing the product was concentrated in vacuo to give **14a** (202 mg, 82%) as a white solid. $[\alpha]_D^{20}$ 43.8 (c = 1.00, 0.1 N NaOH). MS (ES-) 283 $[M-H]^-$. ^{1}H NMR (400 MHz, D_2O, δ): 8.30 (s, 1H), 4.24 (ddd, J = 10, 8.3, 4.4 Hz, 1H), 3.22 (s, 1H), 2.40 (dd, J = 14, 8.1 Hz, 1H), 2.18 (m, 1H), 2.02 (dd, J = 6.5, 3.2 Hz, 1H), 1.54 (t, J = 3.2 Hz, 1H), 1.44 (dd, J = 14, 10 Hz, 1H). ^{13}C NMR (125 MHz, D_2O, δ): 182.2, 181.2, 155.5, 152.9, 65.93, 46.86, 41.63, 37.39, 31.76, 22.96. HRMS ESI (m/z): calcd. for $C_{10}H_{13}N_4O_4S$ $[M+H]^+$: 285.0652. Found: 285.0651. CE, Table S3.

(1*R*,2*S*,4*R*,5*R*,6*R*)-2-Amino-4-[(5-methyl-1*H*-1,2,4-triazol-3-yl)sulfanyl]bicyclo[3.1.0]hexane-2,6-dicarboxylic acid (14b). A suspension of **13b** (85 mg, 0.17 mmol) in 50% aq. acetic acid (2.0 mL) was heated to 160 °C in a microwave for 6 min. The reaction was concentrated in vacuo. The solid was concentrated from water twice to give **14b** (44 mg, 89%) as a white solid. MS (ES+) 299 $[M+H]^+$. ^{1}H NMR (400 MHz, D_2O w/ KOD, δ): 3.92 (m, 1H), 2.10 (dd, J = 14, 8.0 Hz, 1H), 2.07 (s, 3H), 1.90 (m, 1H), 1.81 (m, 1H), 1.52 (t, J = 2.9 Hz, 1H), 1.03 (dd, J = 14, 10 Hz, 1H). . ^{13}C NMR (125 MHz, D_2O, δ): 182.2, 181.2, 162.6, 155.7, 65.95, 46.79, 41.69, 37.38, 31.72, 22.96, 12.33. CE, Table S3.

(1*R*,2*S*,4*R*,5*R*,6*R*)-2-Amino-4-[[5-(trifluoromethyl)-1*H*-1,2,4-triazol-3-yl]sulfanyl]bicyclo[3.1.0]hexane-2,6-dicarboxylic acid hydrochloride (14c). Protected amino acid **13c** (2.47 g, 4.37 mmol) was treated with 4 M HCl in 1,4-dioxane (15 mL, 60 mmol, 20 equiv.) The reaction was stirred at rt overnight, concentrated in vacuo and purified via normal phase chromatography using acetonitrile/0.01 M aq. HCl as the eluent. The purified material was concentrated vacuo to give **14c** (1.1 g, 100%) as the hydrochloride salt. MS (ES+) 353.0 $[M+H]^+$. ^{1}H NMR (400 MHz, D_2O w/ KOD, δ): 4.40 (m, 1H), 2.63 (dd, J = 14, 8.0 Hz, 1H), 2.46 (m, 1H), 2.37 (dd, J = 6.6, 3.2 Hz, 1H), 1.79 (t, J = 3.4 Hz), 1.59 (dd, J = 14, 10 Hz, 1H). ^{19}F NMR (282 MHz, D_2O, δ): -63.71. ^{13}C NMR (125 MHz, D_2O, δ): 182.2, 181.0, 157.66, 154.5 (q, J = 37 Hz, triazole ortho to CF_3), 120.2 (q, J = 267 Hz, CF_3), 65.94, 46.90, 41.53,

37.41, 31.57, 22.98. HRMS ESI (m/z): calcd. for $C_{11}H_{12}F_3N_4O_4S$ $[M+H]^+$: 353.0529. Found: 353.0527. CE, Table S3.

(1*R*,2*S*,4*R*,5*R*,6*R*)-2-Amino-4-[[5-(difluoromethyl)-1*H*-1,2,4-triazol-3-yl]sulfanyl]bicyclo[3.1.0]hexane-2,6-dicarboxylic acid hydrochloride (14d). A solution of protected amino acid **13d** (360 mg, 0.65 mmol) in 1,4-dioxane (1.6 mL) was treated with 4 M HCl in 1,4-dioxane (1.6 mL, 6.5 mmol, 10 equiv.) The reaction was stirred at 50 °C overnight, concentrated in vacuo, and purified via normal phase chromatography using acetonitrile/0.01 M aq. HCl as the eluent. The purified material was concentrated vacuo to give **14d** (200 mg, 93%) as the hydrochloride salt. MS (ES+) 335 $[M+H]^+$. ^{1}H NMR (300 MHz, D_2O, δ): 6.83 (t, J = 53 Hz, 1H), 4.33 (m, 1H), 2.50 (dd, J = 14, 8.1 Hz, 1H), 2.36 (m, 1H), 2.22 (dd, J = 6.2, 3.2 Hz, 1H), 1.68 (t, J = 3.0 Hz, 1H), 1.50 (dd, J = 14, 10 Hz, 1H). ^{19}F NMR (282 MHz, D_2O, δ): -119 (d, J = 54 Hz, 2F). ^{13}C NMR (125 MHz, D_2O, δ): 182.1, 181.1, 158.6 (t, J = 26 Hz, triazole ortho to CF_2), 157.4, 110.2 (t, J = 233 Hz, CF_2), 66.00, 46.90, 41.63, 37.44, 31.66, 23.00. HRMS ESI (m/z): calcd. for $C_{11}H_{13}F_2N_4O_4S$ $[M+H]^+$: 335.0621. Found: 335.0614. CE, Table S3.

(1*R*,2*S*,5*R*,6*R*)-2-Amino-4-[(5-amino-1*H*-1,2,4-triazol-3-yl)sulfanyl]bicyclo[3.1.0]hexane-2,6-dicarboxylic acid (14e). Zinc dibromide (1.69 g, 7.51 mmol, 10 equiv.) was added to a stirred solution of **13e** (384 mg, 0.750 mmol) in DCM (60 mL). The reaction was allowed to stir at rt overnight. The solvent was removed in vacuo and the residue was taken up 2 M HCl and stirred at rt overnight, concentrated in vacuo and purified via cation exchange following **General Procedure B**. The eluent containing the product was concentrated in vacuo to give **14e** (120 mg, 55%) as a colorless, glassy solid. MS (ES+) 300 $[M+H]^+$. ^{1}H NMR (400 MHz, D_2O with 1 drop of Pyr-d_5, δ): 4.21 (m, 1H), 2.42 (dd, J = 14, 8.1 Hz, 1H), 2.21 (m, 1H), 2.05 (dd, J = 6.0, 3.0 Hz, 1H), 1.66 (t, J = 3.0 Hz, 1H), 1.47 (dd, J = 14, 10 Hz, 1H). CE, Table S3.

(1*R*,2*S*,5*R*,6*R*)-2-Amino-4-[(5-isopropyl-1*H*-1,2,4-triazol-3-yl)sulfanyl]bicyclo[3.1.0]hexane-2,6-dicarboxylic acid (14f). A suspension of **13f** (168 mg, 0.281 mmol) in 50% aq. acetic acid (2.8 mL) was heated to 160 °C in a microwave for 6 min. The reaction was concentrated in vacuo. The solid was concentrated from water twice to give **14f** (78 mg, 85%) as a white solid. MS (ES+) 327 $[M+H]^+$. ^{1}H NMR (400 MHz, D_2O w/ 1 drop KOD, δ): 3.95 (m, 1H), 2.84 (sept, J = 6.9 Hz, 1H), 2.12 (dd, J = 14, 8.1 Hz, 1H), 1.91 (m, 1H), 1.83 (m, 1H), 1.76 (m, 1H), 1.55

(m, 1H), 1.08 (d, J = 7.1 Hz, 6H). ^{13}C NMR (125 MHz, D_2O with 1 drop of KOD, δ): 182.3, 181.2, 171.8, 155.3, 46.79, 41.72, 37.36, 31.68, 27.62, 22.95, 21.36, 21.33. CE, Table S3.

(1*R*,2*S*,4*R*,5*R*,6*R*)-2-Amino-4-(1*H*-triazol-4-ylsulfanyl)bicyclo[3.1.0]hexane-2,6-dicarboxylic acid (14g). A solution of fully protected amino acid **13g** (1.87 g, 3.77 mmol) in 4 M HCl in dioxane (20.0 ml, 21 equiv.) and stirred at rt for 22 h. The resultant suspension was concentrated in vacuo and purified via cation exchange following **General Procedure B**. The eluent containing the product was concentrated to give **14g** (958 mg, 79.5%) as a white solid. MS (ES+) 285 $[M+H]^+$. ^{1}H NMR (400 MHz, D_2O, with 1 drop NaOD δ): 8.04, (s, 1H), 4.04 (ddd, J = 10, 8.1, 4.4 Hz, 1H), 2.42 (dd, J = 14, 8.1 Hz, 1H), 2.32 (m, 1H), 2.24 (dd, J = 6.4, 3.2 Hz, 1H), 1.61 (t, J = 3.2 Hz, 1H), 1.46 (dd, J = 14, 10 Hz, 1H). ^{13}C NMR (125 MHz, D_2O with 1 drop of KOD, δ): 182.2, 181.2, 136.6, 133.8, 66.00, 48.10, 41.02, 37.25, 31.87, 22.81. HRMS ESI (m/z): calcd. for $C_{10}H_{13}N_4O_4S$ $[M+H]^+$: 285.0652. Found: 285.0645. CE, Table S3.

Di-*tert*-butyl (1*R*,2*S*,4*S*,5*R*,6*R*)-2-(tert-butoxycarbonylamino)-4-(1*H*-1,2,4-triazol-3-ylsulfanyl)bicyclo[3.1.0]hexane-2,6-dicarboxylate (15a). Following General Procedure A using **12** (27.6 g, 58.0 mmol, 1 equiv.), 1*H*-1,2,4-triazole-3-thiol (7.26 g, 69.6 mmol, 1.20 equiv.), potassium carbonate (16.0 g, 116 mmol, 2.0 equiv.) and DMF (116 mL) the title compound, **15a** (25.3 g, 51.0 mmol), was obtained in 88% yield. MS (ES+) 497.2 $[M+H]^+$. ^{1}H NMR (400 MHz, $CDCl_3$, δ): 8.10 (s, 1H), 5.28 (s, 1H), 4.34 (d, J = 7.7 Hz, 1H), 2.81 (bm, 1H), 2.54 (m, 1H), 2.23 (dd, J = 6.1, 3.2 Hz, 1H), 1.91 (dd, J = 16, 8.3 Hz, 1H), 1.67 (t, J = 3.2 Hz, 1H), 1.52 (s, 9H), 1.43 (s, 9H), 1.42 (s, 9H).

Di-*tert*-butyl (1*R*,2*S*,4*S*,5*R*,6*R*)-2-(tert-butoxycarbonylamino)-4-[(5-methyl-1*H*-1,2,4-triazol-3-yl)sulfanyl]bicyclo[3.1.0]hexane-2,6-dicarboxylate (15b). Following General Procedure A using **12** (220 mg, 0.42 mmol, 1 equiv.), 5-methyl-4*H*-1,2,4-triazole-3-thiol (110 mg, 0.84 mmol, 2.0 equiv.) potassium carbonate (120 mg, 0.84 mmol, 2.0 equiv.) and DMF (2.0 mL). The reaction was then repeated using (636 mg, 1.33 mmol, 1 equiv.), 5-methyl-4*H*-1,2,4-triazole-3-thiol (307 mg, 2.67 mmol, 2.0 equiv.) potassium carbonate (369 mg, 2.67 mmol, 2.0 equiv.) and DMF (6.6 mL). The two batches were combined for work-up and purification to give the title compound **15b** (809 mg) in 90% yield. MS (ES+) 511 $[M+H]^+$. ^{1}H NMR (400 MHz, $CDCl_3$, δ): 10.3 (bs, 1H), 5.14 (bs, 1H), 4.30 (d, J = 8.3 Hz, 1H), 2.88 (bm, 1H), 2.55 (m, 1H), 2.44 (s, 3H),

2.24 (m, 1H), 1.89 (dd, J = 16, 8.3 Hz, 1H), 1.65 (t, J = 3.2 Hz, 1H), 1.53(s, 9H), 1.44 (s, 9H), 1.43 (s, 9H).

Di-*tert*-butyl (1*R*,2*S*,4*S*,5*R*,6*R*)-2-(*tert*-butoxycarbonylamino)-4-[[5-(trifluoromethyl)-4*H*-1,2,4-triazol-3-yl]sulfanyl]bicyclo[3.1.0]hexane-2,6-dicarboxylate (15c). Following General Procedure A using **12** (580 mg, 1.22 mmol, 1 equiv.), 5-(trifluoromethyl)-4*H*-1,2,4-triazole-3-thiol (309 mg, 1.83 mmol, 1.5 equiv.), potassium carbonate (337 mg, 2.44 mmol, 2.0 equiv.), and DMF (3.6 mL) the title compound, **15c** (506 mg, 0.897 mmol), was obtained in 73% yield. MS (ES+) 587.1 $[M+Na]^+$. ^1H NMR (400 MHz, $CDCl_3$, δ): 11.6 (bs, 1H), 5.34 (bs, 1H), 4.44 (d, J = 8.3 Hz, 1H), 2.90 (bm, 1H), 2.47 (bm, 1H), 2.19 (dd, J = 5.9, 2.9 Hz, 1H), 1.92 (dd, J = 16, 8.3 Hz, 1H), 1.74 (t, J = 2.9 Hz, 1H), 1.51 (s, 9H), 1.45 (s, 18H).

Di-*tert*-butyl (1*R*,2*S*,4*S*,5*R*,6*R*)-2-(*tert*-butoxycarbonylamino)-4-[[5-(difluoromethyl)-4*H*-1,2,4-triazol-3-yl]sulfanyl]bicyclo[3.1.0]hexane-2,6-dicarboxylate (15d). Following General Procedure A using **12** (595 mg, 1.25 mmol, 1 equiv.), sodium 5-(difluoromethyl)-4*H*-1,2,4-triazole-3-thiolate (316 mg, 1.62 mmol, 1.3 equiv.), and DMF (3.7 mL) the title compound, **15d** (367 mg, 0.672 mmol), was obtained in 54% yield. Note that no potassium carbonate was used in this example because the sodium thiolate was used instead of the thiol. MS (ES+) 569 $[M+Na]^+$. ^1H NMR (400 MHz, $CDCl_3$, δ): 11.2 (bs, 1H), 6.69 (t, J = 53 Hz, 1H), 5.24 (bs, 1H), 4.45 (d, J = 8.1 Hz, 1H), 2.89 (bm, 1H), 2.47 (bm, 1H), 2.18 (dd, J = 6.0, 3.4 Hz, 1H), 1.90 (dd, J = 16, 8.1 Hz, 1H), 1.72 (t, J = 3.4 Hz, 1H), 1.52 (s, 9H), 1.44 (s, 18H).

Di-*tert*-butyl (1*R*,2*S*,4*S*,5*R*,6*R*)-4-[(5-amino-1*H*-1,2,4-triazol-3-yl)sulfanyl]-2-(*tert*-butoxycarbonylamino)bicyclo[3.1.0]hexane-2,6-dicarboxylate (15e). Following General Procedure A using **11** (500 mg, 1.05 mmol, 1 equiv.), 5-amino-4*H*-1,2,4-triazole-3-thiolate (244 mg, 2.10 mmol, 2.0 equiv.), potassium carbonate (290 mg, 2.10 mmol, 2.0 equiv.), and DMF (5.0 mL) the title compound, **13e** (388 mg, 0.759 mmol), was obtained in 72% yield. MS (ES+) 512.2 $[M+H]^+$. ^1H NMR (400 MHz, $CDCl_3$, δ): 11.7 (bs, 1H), 5.29 (s, 1H), 4.88 (bs, 2H), 4.18 (d, J = 7.8 Hz, 1H), 2.76 (bm, 1H), 2.56 (bm, 1H), 2.23 (dd, J = 5.9, 2.9 Hz, 1H), 1.87 (dd, J = 16, 8.3 Hz, 1H), 1.62 (t, J = 2.6 Hz, 1H), 1.51 (s, 9H), 1.44 (s, 9H), 1.42 (s, 9H).

Di-*tert*-butyl (1*R*,2*S*,4*S*,5*R*,6*R*)-2-(*tert*-butoxycarbonylamino)-4-[(5-isopropyl-4*H*-1,2,4-triazol-3-yl)sulfanyl]bicyclo[3.1.0]hexane-2,6-dicarboxylate (15f). Following General

Procedure A using **11** (556 mg, 1.17 mmol, 1 equiv.), 5-isopropyl-4*H*-1,2,4-triazole-3-thiolate (669 mg, 4.47 mmol, 4.0 equiv.), potassium carbonate (484 mg, 3.50 mmol, 3.0 equiv.), and DMF (9.5 mL) the title compound, **15f** (397 mg, 0.738 mmol), was obtained in 63% yield. MS (ES+) 539 $[M+H]^+$. ^{1}H NMR (400 MHz, $CDCl_3$, δ): 11.0 (bs, 1H), 5.28 (bs, 1H), 4.27 (d, J = 8.1 Hz, 1H), 3.09 (sept., J = 7.0 Hz, 1H), 2.76 (bm, 1H), 2.61 (bm, 1H), 2.27 (m, 1H), 1.90 (dd, J = 16, 8.1 Hz, 1H), 1.65 (t, J = 3.0 Hz, 1H), 1.53 (s, 9H), 1.44 (s, 9H), 1.43 (s, 9H), 1.34 (d, J = 7.0 Hz, 6H).

Di-*tert*-butyl (1*R*,2*S*,4*S*,5*R*,6*R*)-2-(*tert*-butoxycarbonylamino)-4-(1*H*-triazol-5-ylsulfanyl)bicyclo[3.1.0]hexane-2,6-dicarboxylate (15g). Following General Procedure A using **11** (585 mg, 1.23 mmol, 1 equiv.), sodium 1*H*-1,2,3-triazole-5-thiolate dehydrate (302 mg, 2.46 mmol, 2.0 equiv.), and DMF (3.7 mL) the title compound, **15g** (624 mg, 1.23 mmol), was obtained in 100% yield. Note that no potassium carbonate was used in this example because the sodium thiolate was used instead of the thiol. MS (ES+) 497.1 $[M+H]^+$. ^{1}H NMR (400 MHz, $CDCl_3$, δ): 8.05 (s, 1H), 7.68 (bs, 1H), 5.36 (bs, 1H), 3.92 (d, J = 7.8 Hz, 1H), 2.76 (bm, 1H), 2.63 (m, 1H), 2.21 (m, 1H), 1.82 (dd, J = 15, 7.8 Hz, 1H), 1.60 (t, J = 2.9 Hz, 1H), 1.54 (s, 9H), 1.44 (s, 9H), 1.42 (s, 9H).

(1*R*,2*S*,4*S*,5*R*,6*R*)-2-Amino-4-(1*H*-1,2,4-triazol-3-ylsulfanyl)bicyclo[3.1.0]hexane-2,6-dicarboxylic acid (16a). A suspension of **15a** (95 mg, 0.19 mmol) in 50% aq. acetic acid (2.0 mL) was heated to 160 °C in a microwave for 6 min. The reaction was concentrated in vacuo. The solid was concentrated from water twice to give **16a** (55 mg, 100%) as a white solid. MS (ES+) 285 $[M+H]^+$. ^{1}H NMR (400 MHz, D_2O, δ): 8.26 (s, 1H), 4.16 (d, J = 7.7 Hz, 1H), 2.37-2.31 (m, 2H), 2.26 (dd, J = 6.0, 3.0 Hz, 1H), 2.14 (dd, J = 16, 8.5 Hz, 1H), 1.75 (t, J = 3.0 Hz, 1H). ^{13}C NMR (125 MHz, D_2O, δ): 177.4, 174.8, 156.9, 146.5, 66.74, 47.54, 39.42, 34.26, 33.28, 24.98. CE, Table S3.

(1*R*,2*S*,4*S*,5*R*,6*R*)-2-Amino-4-[(5-methyl-1*H*-1,2,4-triazol-3-yl)sulfanyl]bicyclo[3.1.0]hexane-2,6-dicarboxylic acid (16b). Zinc dibromide (3.57 g, 15.84 mmol, 10 equiv.) was added to a stirred solution of **15b** (809 mg, 1.58 mmol) in DCM (130 mL). The reaction was allowed to stir at rt overnight. An additional 5 equiv. of zinc dibromide was added and the reaction allowed to stir overnight. The solvent was removed in vacuo and the residue was taken up 2 M HCl and

stirred at rt overnight, concentrated in vacuo and purified via cation exchange following **General Procedure B**. The eluent containing the product was concentrated in vacuo to give **16b** (357 mg, 76%) as an off-white solid. MS (ES+) 299 $[M+H]^+$. ^{1}H NMR (400 MHz, D_2O w/ KOD, δ): 3.84 (d, J = 7.4 Hz, 1H), 2.18 (d, J = 15 Hz, 1H), 2.16 (s, 3H), 2.12 (dd, J = 5.8, 3.2 Hz, 1H), 1.83 (dd, J = 5.8, 2.5 Hz, 1H), 1.65 (dd, J = 15, 7.6 Hz, 1H), 1.47 (t, J = 2.9 Hz, 1H). ^{13}C NMR (125 MHz, D_2O, δ): 182.5, 181.1, 162.6, 157.0, 66.03, 47.89, 42.26, 34.96, 32.59, 25.47, 12.31. CE, Table S3.

(1*R*,2*S*,4*S*,5*R*,6*R*)-2-Amino-4-[[5-(trifluoromethyl)-1*H*-1,2,4-triazol-3-yl]sulfanyl]bicyclo[3.1.0]hexane-2,6-dicarboxylic acid hydrochloride (16c). Protected amino acid **15c** (506 mg, 0.896 mmol) in 1,4-dioxane (2.2 mL) was treated with 4 M HCl in 1,4-dioxane (2.2 mL, 9.0 mmol, 10 equiv.) The reaction was stirred at 50 °C overnight, concentrated in vacuo and purified via cation exchange following **General Procedure B**. The eluent containing the product was concentrated in vacuo to give still impure product. The material was purified via normal phase chromatography eluting with 100/0 to 85/15 acetonitrile/0.01 M aq. HCl. Fractions containing product were combined and concentrated. The material was purified a second time on normal phase chromatography eluting with 100/0 to 70/30 acetonitrile/0.01 M aq. HCl. Fractions containing pure product were combined and concentrated in vacuo to give **16c** (0.25 g, 72%) as a white solid. MS (ES+) 353.0 $[M+H]^+$. ^{1}H NMR (400 MHz, D_2O w/ KOD, δ): 4.33 (d, J = 8.1 Hz, 1H), 2.58 (m, 1H), 2.55 (d, J = 16, Hz, 1H), 2.46 (dd, J = 6.1, 2.9 Hz, 1H), 2.31 (dd, J = 16, 8.3 Hz, 1H), 2.02 (t, J = 3.4 Hz). ^{13}C NMR (125 MHz, D_2O, δ): 182.5, 181.0, 159.0, 154.4 (q, J = 37 Hz, triazole carbon ortho to CF_3), 120.2 (q, J = 268 Hz, CF_3), 66.03, 48.12, 42.15, 35.04, 32.49, 25.47. HRMS ESI (m/z): calcd. for $C_{11}H_{12}F_3N_4O_4S$ $[M+H]^+$: 353.0529. Found: 353.0523. CE, Table S3.

(*1R,2S,4S,5R,6R*)-2-Amino-4-{[5-(difluoromethyl)-4*H*-1,2,4-triazol-3-yl]sulfanyl}bicyclo[3.1.0]hexane-2,6-dicarboxylic acid hydrochloride (16d). A solution of protected amino acid **15d** (363 mg, 0.664 mmol) in 1,4-dioxane (19 mL) was treated with 4 M HCl in 1,4-dioxane (1.6 mL, 6.6 mmol, 10 equiv.) The reaction was stirred at 50 °C overnight, concentrated in vacuo, and purified via two iterations of normal phase chromatography eluting with a gradient from 100/0 to 80/20 acetonitrile/0.01 M HCl. Clean fractions were combined and concentrated vacuo. The solid was recrystallized in < 2.0 mL of water. The crystals were

collected by vacuum filtration to give **16d** (28 mg, 11%) as the hydrochloride salt. MS (ES+) 335 $[M+H]^+$. ^1H NMR (300 MHz, D_2O, δ): 6.80 (t, J = 53 Hz, 1H), 4.25 (d, J = 8.1 Hz, 1H), 2.39 (m, 1H), 2.38 (d, J = 16 Hz, 1H), 2.33 (dd, J = 6.1, 2.9 Hz, 1H), 2.19 (dd, J = 16, 8.2 Hz, 1H), 1.83 (t, J = 2.9 Hz, 1H). HRMS ESI (m/z): calcd. for $C_{11}H_{13}F_2N_4O_4S$ $[M+H]^+$: 335.0621. Found: 335.0620. CE, Table S3.

(1*R*,2*S*,4*S*,5*R*,6*R*)-2-Amino-4-[(5-amino-1*H*-1,2,4-triazol-3-yl)sulfanyl]bicyclo[3.1.0]hexane-2,6-dicarboxylic acid hydrochloride (16e). Zinc dibromide (1.66 g, 7.37 mmol, 10 equiv.) was added to a stirred solution of **13e** (377 mg, 0.737 mmol) in DCM (60 mL). The reaction was allowed to stir at rt for 3 d. The solvent was removed in vacuo and the residue was taken up 2 M HCl (12 mL) and stirred at rt for 3 d, concentrated in vacuo and purified via cation exchange following **General Procedure B**. The eluent containing the product was concentrated in vacuo to give impure product. The material was purified via normal phase chromatography eluting with 100/0 to 85/15 acetonitrile/0.01 M aq. HCl. Fractions containing pure product were combined and concentrated. The purified material was dissolved in water with 3 drops of 5 N HCl and freeze-dried to give **16e** (91 mg, 37%) as an off-white solid. MS (ES+) 300 $[M+H]^+$. ^1H NMR (400 MHz, D_2O, δ): 4.22 (d, J = 8.6 Hz, 1H), 2.51 (dd, J = 5.6, 3.0 Hz, 1H), 2.46 (d, J = 16 Hz, 1H), 2.42 (dd, J = 5.6, 3.0 Hz, 1H), 2.23 (dd, J = 16, 8.6 Hz, 1H), 1.95 (t, J = 3.0 Hz, 1H). CE, Table S3.

(1*R*,2*S*,4*S*,5*R*,6*R*)-2-Amino-4-[(5-isopropyl-1*H*-1,2,4-triazol-3-yl)sulfanyl]bicyclo[3.1.0]hexane-2,6-dicarboxylic acid hydrochloride (16f). A suspension of **15f** (300 mg, 0.557 mmol) in 50% aq. acetic acid (6.0 mL) was heated to 150 °C in a microwave for 6 min. The reaction was concentrated in vacuo. The solid was concentrated from water three times to remove excess HOAc. The free-base was slurried in water to which was added 1 M HCl (0.5 mL, until solution was obtained). The solution was concentrated in vacuo, redissolved in water and freeze-dried to give **16f** (170 mg, 84%) as a white solid. MS (ES+) 327 $[M+H]^+$. ^1H NMR (400 MHz, D_2O, δ): 3.98 (d, J = 7.6 Hz, 1H), 2.98 (septet, J = 7.1 Hz, 1H), 2.25 (d, J = 15 Hz, 1H), 2.18 (m, 1H), 1.98 (m, 1H), 1.87 (dd, J = 15, 7.6 Hz, 1H), 1.56 (m, 1H), 1.16 (d, J = 7.1 Hz, 6H). ^{13}C NMR (125 MHz, D_2O, δ): 182.6, 181.2, 171.8, 156.5, 66.04, 47.98, 42.24, 34.90, 32.55, 27.64, 25.47, 21.38, 21.32. HRMS ESI (m/z): calcd. for $C_{13}H_{19}N_4O_4S$ $[M+H]^+$: 327.1127. Found: 327.1135. CE, Table S3.

(1*R*,2*S*,4*S*,5*R*,6*R*)-2-Amino-4-(1*H*-triazol-4-ylsulfanyl)bicyclo[3.1.0]hexane-2,6-dicarboxylic acid hydrochloride (16g). A mixture of fully protected amino acid **15g** (350 mg, 0.705 mmol) in 50% aq. acetic acid (10 mL) was heated in a microwave for 6 min at 160 ºC. The reaction was concentrated in vacuo. Water was added and evaporated three times to remove excess acetic acid. The solid was taken up in 2 mL of water. The suspension was treated with 2.5 N NaOH until pH = 7 and all material had dissolved. To the solution was slowly added 5 N HCl until pH = 3 and the zwitterion began to precipitate. After standing overnight the solid was collected via vacuum filtration. The solid (50 mg) was dissolved in 1 mL 0.5 N HCl. After 10 min the solution was concentrated. The solid was dissolved in water and freeze-dried to give **16g** (58 mg, 52%) as an off-white solid. MS (ES+) 285 $[M+H]^+$. ^{1}H NMR (400 MHz, D_2O, δ): 7.97, (s, 1H), 3.86 (d, J = 7.8 Hz, 1H), 2.58 (dd, J = 6.2, 3.2 Hz, 1H), 2.49 (d, J = 16 Hz, 1H), 2.36 (dd, J = 6.2, 3.2 Hz, 1H), 2.16 (dd, J = 16, 7.9 Hz, 1H), 1.92 (t, J = 3.1 Hz, 1H). ^{13}C NMR (125 MHz, D_2O, δ): 174.2, 172.0, 137.3, 130.565.33, 49.12, 38.31, 34.33, 32.73, 22.64. HRMS ESI (m/z): calcd. for $C_{10}H_{13}N_4O_4S$ $[M+H]^+$: 285.0652. Found: 285.0644. CE, Table S3.

Biological Methods

Binding assays: Membranes were prepared either from AV12 cells stably expressing rat glutamate transporter EAAT1 and $mGlu_2$ or $mGlu_3$ or from rat cortex. Compounds were solubilized in 0.1N NaOH as 10 mM stocks, stored at -20 °C, and serially diluted in assay buffer (10 mM potassium phosphate, 100 mM potassium bromide buffer, pH7.6) supplemented with 20 mM HEPES buffer at the start of each experiment. Compounds were tested in a 96-well format in a 3X dilution series to generate a 10-point curve. Diluted compound was incubated with $mGlu_2$ or $mGlu_3$ membranes for 90 min at 25 ºC in the presence of 2 nM **[^{3}H]-7**[28] (18 Ci/mmol). Membranes harvested by filtration and quantified by liquid scintillation counting. Specific binding was calculated as % binding in absence of any inhibitor, corrected for binding in the presence of unlabeled **7**. IC_{50} values were calculated with a four-parameter logistic curve fitting program (ActivityBase v5.3.1.22). Ki values were calculated using standard methods from IC_{50}, K_d and ligand concentrations.

cAMP assays: Agonists: inhibition of forskolin-stimulated cAMP production in cells expressing recombinant $mGlu_2$ (Bmax = 21.8 pmol/mg protein) or $mGlu_3$ (Bmax = 5.3 pmol/mg protein) receptors was assessed using HTRF in AV12 cells stably expressing rat glutamate transporter EAAT1 and $mGlu_2$ or $mGlu_3$. Twenty-four hours before the assay, cells were plated at a density of 8,000-10,000cells per well ($mGlu_2$) or 6,000-8,000 cells per well ($mGlu_3$) in tissue culture treated, 96-well, half-area black plates and incubated in medium containing 250 μM ($mGlu_2$) or 125 μM ($mGlu_3$) of glutamine. Compounds were solubilized in 0.1N NaOH as 10 mM stocks, stored at -20 °C, and serially diluted in assay buffer (Hanks buffered salt solution (HBSS) with 0.1% BSA and 0.5 mM IBMX) supplemented with 20 mM HEPES buffer at the start of each experiment. Compounds were tested in 10-pt concentration response curves using 3-fold serial dilution. The final reaction mixture contained 1 μM forskolin (Sigma F6886) and up to 25 μM of test compound. Reactions were incubated at 37 °C for 20 minutes. DCG-IV was employed as the positive control. After lysis, Cisbio™ detection reagents were incubated at room temp for 1 hour. The HTRF signal (ratio of fluorescence at 665 to 620 nM) was detected with an EnVision plate reader. Raw data were converted to pmole/well of cAMP with a cAMP standard curve generated for each experiment. Relative EC_{50} values were calculated from the top-bottom range of the concentration response curve using a four-parameter logistic curve fitting program (ActivityBase v5.3.1.22). Antagonists: reversal of the inhibition of forskolin-stimulated cAMP production by test compounds is measured using homogeneous time resolved fluorescence technology (HTRF; Cisbio cat # 62AM4PEB). The medium is removed and the cells are incubated with 100 μL cAMP stimulation buffer (STIM) for 30 minutes at 37 °C. STIM buffer contains 500 mL HBSS, 1000 mL DPBS, 0.034% BSA, 1.67 mM HEPES and 500 μM IBMX (Sigma I5879). Compounds are tested in 10-point concentration response curves using 3x serial dilution followed by further 40-fold dilution into STIM buffer. DCG IV (Tocris 0975) serves as the reference agonist. The final reaction mixture contains 1 μM (for $mGlu_2$) or 3 μM (for $mGlu_3$) of forskolin (Sigma F6886), DCG IV at its EC90, and up to 25 μM of test compound. Cells are incubated at 37 °C for 20 minutes. To measure the cAMP levels, cAMP-d2 conjugate and anti-cAMP-cryptate conjugate in lysis buffer are incubated with the treated cells at room temperature for 1 hour ($mGlu_2$) or 1.5 h ($mGlu_3$). The HTRF signal is detected using an EnVision plate reader (Perkin-Elmer) to calculate the ratio of fluorescence at 665 to 620 nm. The raw data are converted to cAMP amount (pmol/well) using a cAMP standard curve

generated for each experiment. Relative IC_{50} values are calculated from the top-bottom range of the concentration response curve using a four-parameter logistic curve fitting program (ActivityBase v5.3.1.22).

$hmGlu_2$ and $hmGlu_3$ Ca^{2+} FLIPR assays: AV12 cells stably expressing rat glutamate transporter EAAT1, $G_{\alpha 15}$ subunit, and $mGlu_2$ (Bmax = 1.35 pmol/mg protein) or $mGlu_3$ (Bmax = 6.1 pmol/mg protein). The co-expression of $G_{\alpha 15}$ expression allows these $G_{i/o}$-coupled receptors to signal through the phospholipase C pathway, resulting in ability to measure receptor activation via transient increases in Ca^{2+} flux.) Twenty-four hours before assay, cells were plated at 85K ($mGlu_2$) or 115K ($mGlu_3$) cells/well into 96-well, black-walled, poly-D-lysine-coated plates and incubated in medium containing 250 μM (for $mGlu_2$) or 125 μM (for $mGlu_3$) of L-glutamine. Compounds were solubilized in 0.1N NaOH as 10 mM stocks, stored at -20 °C, and serially diluted in assay buffer supplemented with 20 mM HEPES buffer at the start of each experiment. Compounds were tested in 10-pt concentration response curves using 3-fold serial dilution. Intracellular calcium levels were monitored before and after the addition of compounds using Fluo-3 AM dye in a FLIPR instrument. The maximal response (EC_{max}) was defined using 100 μM glutamate. Compound effect was measured as max - min peak heights in RFUs corrected for basal fluorescence in the absence of glutamate. Agonist effects quantified as percent stimulation induced by compound alone relative to the maximal glutamate response. All data were calculated as relative EC_{50} values using a four-parameter logistic curve fitting program (ActivityBase v5.3.1.22). Antagonist effects were quantified by calculating the percent inhibition of a response elicited by an EC_{90} concentration of glutamate.

Recombinant mGlu receptor selectivity assays. The activity of test compounds for the other human mGlu receptors were assessed in either FLIPR[36] or cAMP[37] modes using methods analogous to those developed for $mGlu_2$ and $mGlu_3$. Potentiator and antagonist FLIPR assays used a glutamate agonist at levels generating an EC_{10} or EC_{90} response. Antagonist effects were quantified by calculating the % inhibition of the EC_{90} response; potentiation effects were quantified as % increase in the presence of an EC_{10} response relative to the EC_{max} response. The $mGlu_6$ cAMP assays used L-AP4 (Tocris) as the reference agonist. All data were calculated as relative IC_{50} or EC_{50} values using a four-parameter logistic curve fitting program (ActivityBase v5.3.1.22).

Site-Directed Mutants of $mGlu_2$ and $mGlu_3$. Wild-type and mutant mGluRs were generated by PCR, cloned into the pcDNA3.1 vector, and transiently transfected using Fugene HD into AV-12 cells stably expressing the rat glutamate transporter EAAT-1 and the Gα15 subunit. Transfected cells were cultured in DMEM with high glucose supplemented with 5% heat inactivated, dialyzed fetal bovine serum, 1 mM sodium pyruvate, 20 mM HEPES, and 1 mM L-glutamine at 37 ºC in an atmosphere containing 6.5% CO_2 for 48 hours. Cells were harvested and suspended in freeze media (FBS with 6% DMSO) at 10^7cells/ml, and aliquots were stored in liquid nitrogen. Twenty-four hours before the assay, cells were plated at a density of 10,000 cells per well in tissue culture treated, 384-well, black plates in 50 µL of DMEM with high glucose supplemented as above except that only 250 µM of L-glutamine was used. Intracellular calcium levels were monitored before and after the addition of compounds using a Fluorometric Imaging Plate Reader (FLIPR, Molecular Devices). The assay buffer was comprised of Hank's Buffered Salt Solution (HBSS) supplemented with 20 mM HEPES. The medium was removed, and cells were incubated with 25 µL assay buffer containing Calcium-4 dye (Molecular Probes, R8141) for 2 hr at 25 ºC. Compounds were prepared as a 3X dilution series and tested in 10-point concentration curves. A total of 50 fluorescent images were collected. The maximal response was defined as that induced by ECmax (100 µM glutamate). The compound effect was measured as maximal minus minimal peak heights in relative fluorescent units (RFUs) corrected for basal fluorescence measured in the absence of glutamate. Agonist effects were quantified as percent stimulation induced by compound alone relative to the maximal glutamate response. All data were calculated as relative EC_{50} values using a four-parameter logistic curve fitting programs (ActivityBase v5.3.1.22 and GraphPad PRISM v6.03).

Cloning / expression / purification / crystallization $mGlu_2$ and $mGlu_3$ ATDs. All clones were generated by PCR and TOPO-cloned into custom TOPO adapted pFastBac™ vectors (Life Technologies) and sequence verified. Expression in *Sf*9 cells was done with an optimized Bac to Bac™ expression protocol. $mGlu_2$ and $mGlu_3$ are secreted proteins and natural leaders were used. For $mGlu_2$ and $mGlu_3$ secreted media, 1 mL of Ni-NTA resin was added per liter of supernatant and stirred for 2-4 h at 4 °C. The resin was collected and washed with 50 mM Tris HCl (pH 8.0), 500 mM NaCl, 25 mM imidazole, and 10% glycerol. Protein was then eluted with 250 mM imidazole in the same buffer. For $mGlu_2$, samples were further purified by Ni-NTA, size exclusion chromatography, or anion exchange chromatography (depending on sample purity

and amount). For $mGlu_3$, samples were further cleaned by only Ni-NTA. Final samples were concentrated and buffer exchanged with 50 mM Tris pH 8.0 / 150 mM NaCl. The molecular masses of protein samples were determined using matrix assisted laser desorption/ionization (MALDI)-MS (Voyager, DE-RP, Applied Biosystems, Foster City, CA) and a liquid chromatography (LC)-electrospray ionization (ESI) mass spectrometer equipped with a quadrupole time-of-flight mass analyzer (Xevo-Q-TOF, waters Technologies). This information was used to assess both purity and chemical homogeneity, and to compare measured molecular masses to the calculated molecular masses derived from the expected protein sequence. Co-crystals were grown at room temperature using the sitting-drop vapor diffusion method with ~10 mg/mL protein concentration with 5 mM compound in the protein solution and a reservoir solution containing various PEGs and salts. Harvested crystals were cryo-protected using well solution supplemented with 20-25% glycerol, ethylene glycol or PEG400 and flash frozen in liquid nitrogen. Data were collected at Lilly Research Laboratories CAT, sector 31 of the Advanced Photon Source of Argonne National Laboratory. 0.9793 angstrom radiation, using a diamond (111) monchrometer, was used for the data set collected on a Rayonix 225-HE CCD detector. These data were indexed with xds and scaled and truncated using scala and truncate (CCP4). The crystal structures of ligand bound human $mGlu_2$ and human $mGlu_3$ were solved using the separate domains of rat $mGlu_3$ as search models in PHASER. The resulting structure was built using Coot, refined using Buster and validated using MolProbity.

Rat Pharmacokinetics. Compound **14a** was dissolved in water, adjusted to pH of 7−7.5 with NaOH, and administered to fasted male Sprague−Dawley rats (approximately 250 g, Harlan Industries, Indianapolis, IN) at the indicated doses by either oral gavage, intravenous or intraperitoneal route. Serial blood samples (11−12 samples per rat) were collected from a jugular vein catheter into EDTA tubes, centrifuged, and stored frozen until analyzed. Then 25 μL aliquots of thawed plasma were mixed with an equal volume of methanol:water (1:1) containing an analogue internal standard. The mixture was diluted with 300 μL of water and added to a Waters MAX 10 mg SPE plate. The plate was washed with 300 μL of water followed by 300 μL of methanol and the analyte eluted with 400 μL of methanol/formic acid (96:4). Extracts were concentrated, reconstituted in 50 μL of water and analyzed by LCMS/ MS using two Shimadzu LC-20AD pumps (Kyoto, Japan), a Leap PAL autosampler (Carrboro, NC), and a Sciex API 4000 triple quadrupole mass spectrometer (Applied Biosystems/MDS; Foster City, CA)

equipped with a TurboIonSpray interface, and operated in positive ion mode. Chromatographic separation was accomplished on a 2.1 mm × 50 mm, 5 μm BioBasic AX HPLC column (Thermo Scientific, Pittsburgh, PA) using a binary step gradient. The initial mobile phase system was composed of methanol/water (40:60, v/v; mobile phase A) and glacial acetic acid/water (25:75, v/v; mobile phase B). The step gradient profile changed from 1% B for 0.2 min, 35% B at 0.30−0.40 min, 60% B at 0.50 min, and returning to 1% B at 0.76 min. The flow rate was 1.0 mL/min and the column was at ambient temperature, with flow directed to the mass spectrometer between 0.27 and 0.5 min. The selected reaction monitoring (M + H)+ transition was m/z 204.1 > 77.1. Pharmacokinetic parameters were calculated by noncompartmental analysis using Watson 7.4 (Thermo Fischer Scientific).

Rat cerebral spinal fluid pharmacokinetics: Male Sprague Dawley rats (Harlan Industries, Indianapolis, IN) were used for all experiments. Rats had free access to food and water at all times. Compound **14a** was prepared by dissolution in 1 μL of 5 N NaOH per mg followed by addition of water for a dose volume of 1 mL/kg. The pH was checked for neutrality prior to injection. All drugs were administered by the intraperitoneal route at doses of 1, 3 and 10 mg/kg. Plasma and csf were collected at 0.5, 1, and 4 hours post-dosing, the latter being collected via syringe from the cisterna magna. Plasma and csf were stored at -70 ºC until analyzed as described above.

Rat phencyclidine (PCP)-induced locomotor assay: Male Sprague Dawley rats, (7-9 weeks, 225-250 grams, Harlan Industries, Indianapolis, IN) were used for all experiments (sample sizes of 7-8 per group). Rats were housed on a 12:12 light-dark cycle (lights on at 0600) with food and water freely available. Testing occurred during the light phase of the cycle. Motor activity was measured by placing individual rats in a transparent, plastic shoe-box cage of the dimensions 45 x 25 x 20cm, with 1 cm depth of wood chips as bedding, and a metal grill or plastic lid is on top of the cage. Activity monitors (Kinder Scientific) consisted of a rectangular rack of 12 photobeams arranged in an 8 x 4 formation, (or a high density grouping of 22 in a 15x7 pattern) at a height of 5 cm, with a second rack (for measuring rearing behaviors) at a height of 15 cm. Each shoe box cage was placed inside of a rack, resting on a 3 foot high tabletop in an isolated room. Test compounds were dissolved in deionized water with dropwise addition of 5M NaOH

to achieve a pH 7-8 with sonication and administered by intraperitoneal route to rats which had been fasted overnight, then placed in the test cage and allowed to acclimate for 30 minutes prior to the PCP challenge. Two hours after test compound dosing and acclimation, PCP-HCl (5 mg/kg, s.c.) was administered and the rat placed back in the cage for an additional 60 min while activity was measured. Data analysis was performed using GraphPad Prizm (San Diego CA USA). A 1 way ANOVA analysis of variance with a post-hoc Dunnetts multiple comparison test was calculated. When performing the ED_{50} calculation of dose response generated data, dose levels were converted to log values and activity calculated to percent reversals of stated doses. A non-linear regression curve fit with a sigmoidal dose response variable slope analysis was then performed.

Rat rotarod performance assay: The ability of the compound to affect neuromuscular coordination was examined using an accelerating rotarod test. All rats received three training trials to maintain posture on the rotarod accelerating to 17 rpm in 5 seconds and maintaining speed for 40 seconds (Omnitech Electronics Inc, Columbus, OH), prior to the actual day of drug testing. On the following day, rotarod testing was conducted on 8 male Sprague Dawley rats (6-8 weeks, 200-240 grams, Harlan Industries, Indianapolis, IN) per dose at different time points (1, 2, and 3 hours) following intraperitoneal injection of drug or vehicle. Animals that did not fall off the rotarod were given a maximum score of 40 seconds. All rats were given up to 3 trials (single trial = 40 seconds at 17 rpm) to maintain posture on the rod. The best time achieved after 3 trials was recorded for that particular rat/time point and used in data calculations. Rotarod data were evaluated by calculation of mean and standard error for each treatment as well as experimental design-appropriate statistics (Product-Limit Survival Fit Test) which are then used to determine statistical significance of outcome (Wilcoxon Chi Square) using JMP (v 6.0) statistical analysis program (SAS Institute Inc, Cary, NC). Differences were considered to be significant if the p-value was less than 0.05. Data are presented as means with standard errors of means (± SEM).

Animal Studies

All studies involving the use of laboratory animals were consistent with the guidelines for Ethical Treatment of Research Animals published by the American Veterinary Medical Association and approved by the Institutional Animal Care and Use Committee (IACUC) at Lilly Research Laboratories.

Associated Content

Supporting Information: Relationship of $hmGlu_2$ and $hmGlu_3$ affinity for **14a-g, 16a-g**. Calculated thiotriazole NH pKa values for **14a-g, 16a-g**. Relationship of $hmGlu_2$ cAMP and FLIPR agonist potency for **14a-g, 16a-g**. Relationship of $hmGlu_2$ affinity and functional potency for **14a-g, 16a-g**. Relationship of $hmGlu_3$ affinity and cAMP agonist potency for **14a-g, 16a-g**. Extended selectivity assessment for compound **14a**. Chemical structures of **17** and **18**. Crystal structures of **14a** bound to $hmGlu_2$ and $hmGlu_3$ ATDs. Crystal structures of glutamate bound to $hmGlu_2$ and $hmGlu_3$ ATDs; Agonist responses of **18** in WT and mutant $hmGlu_2$ and $hmGlu_3$ receptors (reproduced from reference 25). Capillary electrophoresis based purity results for **14a-g**, **16a-g** and CE trace for **14a**. This material is available free of charge via the Internet at http://pubs.acs.org.

Acknowledgement

This research used resources of the Advanced Photon Source, a U.S. Department of Energy (DOE) Office of Science User Facility operated for the DOE Office of Science by Argonne National Laboratory under Contract No. DE-AC02-06CH11357. Use of the Lilly Research Laboratories Collaborative Access Team (LRL-CAT) beamline at Sector 31 of the Advanced Photon Source was provided by Eli Lilly Company, which operates the facility.

Author Information

Corresponding Author

*Phone: 317-276-9101. Email: monn@lilly.com

Disclosures

All authors were employed by Eli Lilly and Company during time this research was conducted, and all funding for the work was provided by Eli Lilly and Company. The authors declare no competing financial interests.

Abbreviations Used

ATD, amino terminal domain; C_0, plasma concentration after iv dosing extrapolated to $t = 0$; C_{max}, peak plasma concentration after oral dosing; CL, iv clearance; csf, cerebrospinal fluid; cAMP, 3'-5'-cyclic adenosine monophosphate; DAST, diethylaminosulfur trifluoride; FLIPR, fluorescence imaging plate reader; HTRF, Homogenous time resolved fluorescence; mGlu, metabotropic glutamate; PCP, 1-phenylcyclohexylpiperidine; *Si*-DMT, SiliaMetS® Dimercaptotriazine; Si-Triamine, SiliaMetS® Triamine; $V_{d\ ss}$, volume of distribution at steady state.

PDB ID Codes

$hmGlu_2$ ATD with LY2812223 (**14a**): 5CNJ; $hmGlu_3$ ATD with LY2812223 (**14a**): 5CNM; $hmGlu_2$ ATD with L-glutamate: 5CNI; $hmGlu_3$ ATD with L-glutamate: 5CNK

References

1. (a) O'Neill, M. J.; Fell, M. J.; Svensson, K. A.; Witkin, J. M.; Mitchell, S. N. Recent developments in metabotropic glutamate receptors as novel drug targets. *Drugs Future* **2010**, *35*, 307-324. (b) Niswender, C. M.; Conn, P. J. Metabotropic glutamate receptors: physiology, pharmacology, and disease. *Annu. Rev. Pharmacol. Toxicol.* **2010**, *50*, 295-322. (c) Julio-Pieper, M.; Flor, P. J.; Dinan, T. G.; Cryan, J. F. Exciting times beyond the brain: metabotropic glutamate receptors in peripheral and non-neural tissues. *Pharmacol. Rev.* **2011**, *63*, 35-58.
2. (a) Chaki, S. Group II metabotropic glutamate receptor agonists as a potential drug for schizophrenia. *Eur. J. Pharmacol.* **2010**, *639*, 59-66. (b) Sanacora, G.; Zarate, C. A.; Krystal, J. H.; Manji, H. K. Targeting the glutamatergic system to develop novel, improved therapeutics for mood disorders. *Nat. Rev. Drug Discovery* **2008**, *7*, 426-437. (c) Witkin, J. M.; Marek, G. J.; Johnson, B. G.; Schoepp, D. D. Metabotropic glutamate receptors in the control of mood disorders. *CNS Neurol. Disord.: Drug Targets* **2007**, *6*, 87-100.
3. (a) Simmons, R. M. A.; Webster, A. A.; Kalra, A. B.; Iyengar, S. Group II mGluR receptor agonists are effective in persistent and neuropathic pain models in rats. *Pharmacol.; Biochem. Behav.* **2002**, *73*, 419–427. (b) Du, J.; Zhou, S.; Carlton, S. M. Group II metabotropic glutamate receptor activation attenuates peripheral sensitization in inflammatory states. *Neuroscience* **2008**, *154,* 754–766. (c) Kingston, A. E.; O'Neill, M. J.; Lam, A.; Bales, K. R.; Monn, J. A.; Schoepp, D. D. Neuroprotection by metabotropic glutamate receptor agonists: LY354740, LY379268 and LY389795. *Eur. J. Pharmacol.* **1999**, *377*, 155-165. (d) Battaglia, G.; Busceti, C. L.; Pontarelli, F.; Biagioni, F.; Fornai, F.; Paparelli, A.; Bruno, V.; Ruggieri, S.; Nicoletti, F. Protective role of group-II metabotropic glutamate receptors against nigro-striatal degeneration induced by 1-methyl-4-phenyl-1,2,3,6-tetrahydropyridine in mice. *Neuropharmacology* **2003**, *45*, 155-166. (e) Schiefer, J.; Sprunken, A.; Puls, C.; Luesse, H.-G.; Milkereit, A.; Milkereit, E.; Johann, V.; Kosinski, C. M. The metabotropic glutamate receptor 5 antagonist MPEP and the mGluR2 agonist LY379268 modify disease progression in a transgenic mouse model of Huntington's disease. *Brain Res.* **2004**, *1019*, 246-254. (f) Garcia, B. G.; Neely, M. D.; Deutch, A.

Y. Cortical regulation of striatal medium spiny neuron dendritic remodeling in parkinsonism: modulation of glutamate release reverses dopamine depletion-induced dendritic spine loss. *Cereb. Cortex* **2010**, *20*, 2423-2432.

4. (a) Arcella, A.; Carpinelli, G.; Battaglia, G.; D'Onofrio, M.; Santoro, F.; Ngomba, R. T.; Bruno, V.; Casolini, P.; Giangaspero,F.; Nicoletti, F. Pharmacological blockade of group II metabotropic glutamate receptors reduces the growth of glioma cells in vivo *Neuro-oncology* **2005**, 236-245. (b) Ciceroni, C.; Arcella, A.; Mosillo, P.; Battaglia, G.; Mastrantoni, E.; Oliva, M. A.; Carpinelli, G.; Santoro, F.; Sale, P.; Ricci-Vitiani, L.; De Maria, R.; Pallini, R.; Giangaspero, F.; Nicoletti, F.; Melchiorri, D. Type-3 metabotropic glutamate receptors negatively modulate bone morphogenetic protein receptor signaling and support the tumourigenic potential of glioma-initiating cells. *Neuropharmacology* **2008**, *55*, 568–576.
5. (a) Monn, J. A.; Valli, M. J.; Massey, S. M.; Wright, R. A.; Salhoff, C. R.; Johnson, B. G.; Howe, T.; Alt, C. A.; Rhodes, G. A.; Robey, R. L.; Griffey, K. R.; Tizzano, J. P.; Kallman, M. J.; Helton, D. R.; Schoepp, D. D. Design, synthesis and pharmacological characterization of (+)-2-aminobicyclo[3.1.0]hexane-2,6-dicarboxylic Acid (LY354740): a potent, selective and orally active group 2 metabotropic glutamate receptor agonist possessing anticonvulsant and anxiolytic properties. *J. Med. Chem.* **1997**, *40*, 528-537. (b) Schoepp, D. D.; Johnson, B. G.; Wright, R. A.; Salhoff, C. R.; Mayne, N. G.; Wu, S.; Cockerham, S. L.; Burnett, J. P.; Belagaje, R.; Bleakman, D.; Monn, J. A. LY354740 is a potent and highly selective group II metabotropic glutamate receptor agonist in cells expressing human glutamate receptors. *Neuropharmacol*ogy **1997**, *36*, 1-11.
6. (a) Monn, J. A.; Valli, M. J.; Massey, S. M.; Henry, S. S.; Stephenson, G. A.; Bures, M.; Herin, M.; Catlow, J.; Giera, D.; Wright, R. A.; Johnson, B. G.; Andis, S. L.; Kingston, A. E.; Schoepp, D. D. Synthesis and metabotropic glutamate receptor activity of S-oxidized variants of LY389795: Identification of potent, selective and orally bioavailable agonists for mGlu2/3 receptors. *J. Med. Chem.* **2007**, *50,* 233-240. (b) Rorick-Kehn, L. M.; Johnson, B. G.; Burkey, J. L.; Wright, R. A.; Calligaro, D. O.; Marek, G. J.; Nisenbaum, E. S.; Catlow, J. T.; Kingston, A. E.; Monn, J. A.; McKinzie, D. L.; Schoepp, D. D. Pharmacological and pharmacokinetic properties of a

structurally-novel, potent, selective mGlu2/3 receptor agonist: In vitro characterization of LY404039 *J. Pharmacol. Exp. Ther*. **2007**, *321*, 308-317. (c) Rorick-Kehn, L. M.; Johnson, B. G.; Knitowski, K. M.; Salhoff, C. R.; Witkin, J. M.; Perry, K. W.; Griffey, K. I.; Tizzano, J. P.; Monn, J. A.; McKinzie, D. L.; Schoepp, D. D. In vivo pharmacological characterization of the structurally novel, potent, selective mGlu2/3 receptor agonist LY404039 in animal models of psychiatric disorders. *Psychopharmacology* **2007,** *193,* 121-136.

7. Dunayevich, E.; Erickson, J.; Levine, L.; Landbloom, R.; Schoepp, D. D.; Tollefson, G. D. Efficacy and Tolerability of an mGlu2/3 Agonist in the treatment of generalized anxiety disorder. *Neuropsychopharmacology* **2007**, *33*, 1–8.
8. Patil, S. T.; Zhang, L.; Martenyi, F.; Lowe, S. L.; Jackson, K. A.; Andreev, B. V.; Avedisova, A. S.; Bardenstein, L. M.; Gurovich, I. Y.; Morozova, M. A.; Mosolov, S. N.; Neznanov, N. G.; Reznik, A. M.; Smulevich, A. B.; Tochilov, V. A.; Johnson, B. G.;. Monn, J. A.; Schoepp, D. D. Activation of mGlu2/3 receptors as a new approach to treat schizophrenia: a randomized Phase 2 clinical trial. *Nat. Med.* **2007**, *13,* 1102-1107. (b) Mezler, M.; Geneste, H.; Gault, L.; Marek, G. J. LY-2140023, a prodrug of the group II metabotropic glutamate receptor agonist LY-404039 for the potential treatment of schizophrenia. *Curr. Opin. Invest. Drugs* **2010**, *11*, 833-845.
9. (a) Kinon, B. J.; Zhang, L.; Millen, B. A.; Osuntokun, O. O.; Williams, J. E.; Kollack-Walker, S.; Jackson, K.; Kryzhanovskaya, L.; JarKova, N.; and the HBBI Study Group. A multicenter, inpatient, phase 2, double-blind, placebo-controlled dose-ranging study of LY2140023 monohydrate in patients with DSM-IV schizophrenia. *J. Clin. Psychopharmacol*. **2011**, *31*, 349-355. (b) Kinon B. J. Development of Pomaglumetad Methionil (LY2140023) as an Innovative Glutamate-based Pharmacotherapy for Schizophrenia. Presented at the ACNP 52nd Annual Meeting Hollywood, FL, Dec 8-12, 2013 (c) Liu, W.; Downing, A. C. M.; Munsie, L. M.; Chen, P.; Reed, M. R.; Ruble, C. L.; Landschulz, K. T.; Kinon, B. J.; Nisenbaum, L. K. Pharmacogenetic analysis of the mGlu2/3 agonist LY2140023 monohydrate in the treatment of schizophrenia. *Pharmacogenomics J.* **2012**, *12*, 246-254. (d) Kinon, B. J.; Millen, B. A.; Zhang, L.; McKinzie, D. L. Exploratory analysis for a targeted population responsive to the metabotropic glutamate 2/3 agonist pomaglumetad

methionil in schizophrenia. *Biol. Psych*. **2015**, in press (http://dx.doi.org/10.1016/j.biopsych.2015.03.016).

10. (a) Gu, G.; Lorrain, D. S.; Wei, H.; Cole, R. L.; Zhang, X.; Daggett, L. P.; Schaffhauser, H.; Bristow L. J.; Lechner, S. M. Distribution of metabotropic glutamate 2 and 3 receptors in the rat forebrain: Implication in emotional responses and central disinhibition. *Brain Res*. **2008**, *1197*, 47-62. (b) Tamaru, Y.; Nomura, S.; Mizuno N.; Shigemoto R. Distribution of metabotropic glutamate receptor mGluR3 in the mouse CNS: Differential location relative to pre- and postsynaptic sites. *Neuroscience* **2001**, *106,* 481-503.
11. Linden, A.-M.; Shannon, H.; Baez, M.; Yu, J. L.; Koester, A.; Schoepp, D. D. Anxiolytic-like activity of the mGlu2/3 receptor agonist LY354740 in the elevated plus maze test is disrupted in metabotropic glutamate receptor 2 and 3 knockout mice. *Psychopharmacology* **2005**, *179*, 284-291.
12. (a) Spooren, W. P. J. M.; Gasparini, F.; van der Putten, H.; Koller, M.; Nakanishi, S.; Kuhn R. Lack of effect of LY314582 (a group 2 metabotropic glutamate receptor agonist) on phencyclidine-induced locomotor activity in metabotropic glutamate receptor 2 knockout mice. *Eur. J. Pharmacol.* **2000**, *397*, R1-R2. (b) Fell, M. J.; Svensson, K. A.; Johnson, B. G.; Schoepp, D. D. Evidence for the role of metabotropic glutamate (mGlu)2 not mGlu3 receptors in the preclinical antipsychotic pharmacology of the mGlu2/3 receptor agonist(-)-(1*R,*4*S*,5*S*,6*S*)-4-amino-2-sulfonylbicyclo[3.1.0]hexane-4,6-dicarboxylic acid (LY404039). *J. Pharmacol. Exp. Ther.* **2008**, *326*, 209-217.
13. Zammataro, M.; Chiechio, S.; Montana, M. C.; Traficante, A.; Copani, A.; Nicoletti, F.; Gereau, R. W. mGlu2 metabotropic glutamate receptors restrain inflammatory pain and mediate the analgesic activity of dual mGlu2/mGlu3 receptor agonists. *Mol. Pain* **2011**, *7*, 6-10.
14. Aronica, E.; Gorter, J. A.; Ijlst-Keizers, H.; Rozemuller, A. J.; Yankaya, B.; Leenstra, S.; Troost, D. Expression and functional role of mGluR3 and mGluR5 in human astrocytes and glioma cells: opposite regulation of glutamate transporter proteins. *Eur. J. Neurosci.* **2003**, *17*, 2106-2118.

15. (a) Corti, C.; Battaglia, G.; Molinaro, G.; Riozzi, B.; Pittaluga, A.; Corsi, M.; Mugnaini, M.; Nicoletti, F.; Bruno, V. The use of knock-out mice unravels distinct roles for mGlu2 and mGlu3 metabotropic glutamate receptors in mechanisms of neurodegeneration/neuroprotection. *J. Neurosci.* **2007**, *27*, 8297-8308. (b) Battaglia, G.; Molinaro, G.; Riozzi, B.; Storto, M.; Busceti, C. L.; Spinsanti, P.; Bucci, D.; Di Liberto, V.; Mudo, G.; Corti, C.; Corsi, M.; Nicoletti, F.; Belluardo, N.; Bruno, V. Activation of striatal mGlu3 receptors stimulates the production of GDNF in striatal neurons. *PLoS One*, **2009**, *4*, e6591. (c) Battaglia, G.; Riozzi, B.; Bucci, D.; Di Menna, L.; Molinaro, G.; Pallottino, S.; Nicoletti, F.; Bruno, V. Activation of mGlu3 metabotropic glutamate receptors enhances GDNF and GLT-1 Formation in the spinal cord and rescues motor neurons in the SOD-1 mouse model of amyotrophic lateral sclerosis. *Neurobiol. Dis.* **2014**, *74*, 126-136.

16. Ster, J.; Mateos, J. M.; Grewe, B. F.; Coiret, G.; Corti, C.; Corsi, M.; Helmchen, F.; Gerber, U. Enhancement of CA3 hippocampal network activity by activation of group II metabotropic glutamate receptors. *Proc. Nat. Acad. Sci. U.S.A.* **2011**, *108*, 9993-9997.

17. Walker, A. G.; Wenthur, C. J.; Xiang, Z.; Rook, J. M.; Emmitte, K. A.; Niswender, C. M.; Lindsley, C. W.; Conn, P. J. Metabotropic glutamate receptor 3 activation is required for long-term depression in medial prefrontal cortex and fear extinction. *Proc. Nat. Acad. Sci. U.S.A.* **2015**, *112*, 1196-1201.

18. Lyon, L.; Kew, J. N. C.; Corti, C.; Harrison, P. J.; Burnet, P. W. J. Altered hippocampal expression of glutamate receptors and transporters in GRM2 and GRM3 knockout mice. *Synapse* **2008**, *62*, 842-850.

19. Tanabe, Y.; Masu, M.; Ishii, T.; Shigemoto R.; Nakanishi, S. A family of metabotropic glutamate receptors. *Neuron* **1992,** *8,* 169-179.

20. (a) Muto, T.; Tsuchiya, D.; Morikawa, K.; Jingami, H. Structures of the extracellular regions of the group II/III metabotropic glutamate receptors. *Proc. Natl. Acad. Sci. U. S. A.* **2007**, *104*, 3759-3764. (b) Wernimont, A. K.; Dong, A.; Seitova, A.; Crombet, L.; Khutoreskaya, G.; Edwards, A. M.; Arrowsmith, C. H.; Bountra, C.; Weigelt, J.; Cossar, D.; Dobrovetsky, E. Crystal structure of metabotropic glutamate receptor 3

precursor in presence of LY341495 antagonist. RCSB protein data bank DOI:10.2210, PDB3SM9, deposited June 27, 2011.

21. (a) Fraley, M. E. Positive allosteric modulators of the metabotropic glutamate receptor 2 for the treatment of schizophrenia. *Expert Opin. Ther. Pat*. **2009**, *19*, 1-17. (b) Trabanco, A. A.; Cid, J. M.; Lavreysen, H.; MacDonald, G. J.; Tresadern, G. Progress in the development of positive allosteric modulators of the metabotropic glutamate receptor 2. *Curr. Med. Chem*. **2011**, *18*, 47-68.
22. Dominguez, C.; Prieto, L.; Valli, M. J.; Massey, S. M.; Bures, M.; Wright, R. A.; Johnson, B. G.; Andis, S. L.; Kingston, A.; Schoepp D. D.; Monn, J. A. Methyl substitution of 2-aminobicyclo[3.1.0]hexane-2,6-dicarboxylate (LY354740) determines functional activity at metabotropic glutamate receptors: Identification of a subtype selective mGlu2 receptor agonist. *J. Med. Chem.* **2005**, *48,* 3605-3612.
23. Nielsen, S. D.; Fulco, M.; Serpi, M.; Nielsen, B.; Hansen, M. B.; Hansen, K. L.; Thomsen, C.; Brodbeck, R.; Bräuner-Osborne, H.; Pellicciari, R.; Norrby, P.-O.; Greenwood, J. R.; Clausen, R. P. A highly selective agonist for the metabotropic glutamate receptor mGluR2. *Med. Chem. Commun.* **2011**, *2*, 1120-1124.
24. Monn, J. A.; Valli, M. J.; Massey, S. M.; Hao, J.; Reinhard, M.; Bures, M. G.; Heinz, B.; Wang, X.; Carter, J. H.; Getman, B. G.; Stephenson, G. A.; Herin, M.; Catlow, J. T.; Swanson, S.; Johnson, B. G.; Henry S. S. Synthesis and pharmacological characterization of 4-substituted-2-aminobicyclo[3.1.0]hexane-2,6-dicarboxylates: identification of new potent and selective metabotropic glutamate 2/3 receptor agonists. *J. Med. Chem.* **2013**, *56*, 4442-4455.
25. Monn, J. A.; Prieto, L.; Taboada, L.; Hao, J.; Reinhard, M. R.; Henry, S. S.; Beadle, C.; Walton, L.; Man, T.; Rudyk, H.; Clark, B.; Tupper, D.; Baker, S. R.; Lamas, C.; Montero, C.; Marcos, A.; Blanco, J.; Bures, M.; Clawson, D. K.; Atwell, S.; Lu, F.; Wang, J.; Russell, M.; Heinz, B.; Wang, X.; Carter, J.; Getman, B.; Catlow, J.; Swanson, S.; Sanger, H.; Broad, L. M.; Johnson, B. G.; Shaw, D.; McKinzie, D. L. Synthesis and pharmacological characterization of C4-disubstituted analogs of 1S,2S,5R,6S-2-aminobicyclo[3.1.0]hexane-2,6-dicarboxylate: Identification of a potent, selective metabotropic glutamate receptor agonist and determination of agonist-

bound human mGlu2 and mGlu3 amino terminal domain structures. *J. Med. Chem.* **2015**, *58*, 1776-1794.

26. Henry, S. S.; Brady, M. D.; Laird, D. T.; Ruble, J. C.; Varie, D. L; Monn, J. A. Improved Synthesis of $C4_{\alpha}$- and $C4_{\beta}$-Methyl Analogues of 2-Aminobicyclo[3.1.0]hexane-2,6-dicarboxylate. *Org. Lett.* **2012**, *14*, 2662-2665.
27. See experimental section for details
28. (a) Kuo, F.; Kulanthaivel, P.; Rener, G. A.; Wheeler, W. J.; Yi, P. Synthesis of LY455169-[$^2H_2$], a model study for the tritium labeling of LY459477. 2. Synthesis of LY459477-[$^3H_2$]. In *Synthesis and Applications of Isotopically Labeled Compounds, Proceedings of the International Symposium, Volume 8*; D. C. Dean, C. N. Filer and K. E. McCarthy, Eds.; John Wiley and Sons, Ltd.: Chichester, UK, 2003; pp. 267-270. (b) Wright, R. A.; Johnson, B. G.; Zhang, C.; Salhoff, C.; Kingston, A. E.; Calligaro, D. O.; Monn, J. A.; Schoepp, D. D.; Marek, G. J. CNS distribution of metabotropic glutamate 2 and 3 receptors: Transgenic mice and [3H]LY459477 autoradiography. *Neuropharmacol*ogy **2013**, *66*, 89-98.
29. pKa values were calculated using MarvinSketch (version 5.8.3) program in ChemAxon
30. Monn, J. A.; Prieto, L.; Taboada Marinez, L.; Montero Salgado, C.; Shaw, B. W. MGlu2 agonists. U.S. Pat. 8,318,184, November 27, 2012.
31. Molecular Operating Environment (MOE), 2013.08; Chemical Computing Group Inc.; 1010 Sherbooke St. West, Suite #910, Montreal, QC, Canada, H3A 2R7, **2013**.
32. Kingston, A. E.; Ornstein, P. L.; Wright, R. A.; Johnson, B. G.; Mayne, N. G.; Burnett, J. P.; Belagaje, R.; Wu, S.; Schoepp, D. D. LY341495 is a nanomolar potent and selective antagonist of group II metabotropic glutamate receptors. *Neuropharmacology* **1999**, *37*, 1-12.
33. The open angle of the $mGlu_2$ ATD in the presence of compound **14a** is defined by points associated with the Cα atoms of G451 (hinge), Y144 (LB1) and R271 (LB2). For $mGlu_3$, these correspond to G439 (hinge), Y150 (LB1) and R277 (LB2).
34. Kleywegt, G. J.; Jones, T. A. Detecting folding motifs and similarities in protein structures. *Methods in Enzymol.* **1997**, *277*, 525-545.
35. Monn, J. A.; Valli, M. J.; Massey, S. M.; Hansen, M. M.; Kress, T. J.; Wepsiec, J. P.; Harkness, A. R.; Grutsch, J. L. Jr.; Wright, R. A.; Johnson, B. G.; Andis, S. L.;

Kingston, A. E.; Tomlinson, R.; Lewis, R.; Griffey, K. R.; Tizzano, J. P.; Schoepp, D. D. Synthesis, pharmacological characterization and molecular modeling of heterobicyclic amino acids related to LY354740: Identification of LY379268 and LY389795: Two new potent, selective and systemically active agonists for group II metabotropic glutamate receptors. *J. Med. Chem.* **1999**, *42,* 1027-1040.

36. Gilmour, G.; Broad, L. M.; Wafford, K. A.; Britton, T.; Colvin, E. M.; Fivush, A.; Gastambide, F.; Getman, B.; Heinz, B. A.; McCarthy, A. P.; Prieto, L.; Shanks, E.; Smith, J. W.; Taboada, L.; Edgar, D. M.; Tricklebank, M. D. In vitro characterization of the novel positive allosteric modulators of the mGlu5 receptor, LSN2463359 and LSN2814617, and their effects on sleep architecture and operant responding in the rat. *Neuropharmacology* **2013**, *64*, 224-239.
37. Wu, S.; Wright, R. A.; Rockey, P. K.; Burgett, S. G.; Arnold, J. S.; Rosteck, P. R. Jr.; Johnson, B. G.; Schoepp, D. D.; Belagaje, R. Group III human metabotropic glutamate receptors 4, 7 and 8: "Molecular cloning, functional expression, and comparison of pharmacological properties in RGT cells" *Mol. Brain Res.* **1998**, *53*, 88-97.

TOC Graphic